

# Was Einstein Right? A Centenary Assessment

Clifford M. Will  
Department of Physics  
University of Florida  
Gainesville FL 32611 U.S.A.

This article is an overview of 100 years of testing general relativity, to be published in the book *General Relativity and Gravitation: A Centennial Perspective*, to commemorate the 100th anniversary of general relativity. It is effectively an abridged version of the recent update of the author's *Living Review in Relativity*.

## I. INTRODUCTION

When general relativity was born 100 years ago, experimental confirmation was almost a side issue. Admittedly, Einstein did calculate observable effects of general relativity, such as the perihelion advance of Mercury, which he knew to be an unsolved problem, and the deflection of light, which was subsequently verified. But compared to the inner consistency and elegance of the theory, he regarded such empirical questions as almost secondary. He famously stated that if the measurements of light deflection disagreed with the theory he would “feel sorry for the dear Lord, for the theory *is* correct!”.

By contrast, today at the centenary of Einstein's towering theoretical achievement, experimental gravitation is a major component of the field, characterized by continuing efforts to test the theory's predictions, both in the solar system and in the astronomical world, to detect gravitational waves from astronomical sources, and to search for possible gravitational imprints of phenomena originating in the quantum, high-energy or cosmological realms.

The modern history of experimental relativity can be divided roughly into four periods: Genesis, Hibernation, a Golden Era, and the Quest for Strong Gravity. The Genesis (1887–1919) comprises the period of the two great experiments which were the foundation of relativistic physics – the Michelson–Morley experiment and the Eötvös experiment – and the two immediate confirmations of general relativity – the deflection of light and the perihelion advance of Mercury. Following this was a period of Hibernation (1920–1960) during which theoretical work temporarily outstripped technology and experimental possibilities, and, as a consequence, the field stagnated and was relegated to the backwaters of physics and astronomy.

But beginning around 1960, astronomical discoveries (quasars, pulsars, cosmic background radiation) and new experiments pushed general relativity to the forefront. Experimental gravitation experienced a Golden Era (1960–1980) during which a systematic, world-wide effort took place to understand the observable predictions of general relativity, to compare and contrast them with the predictions of alternative theories of gravity, and to perform new experiments to test them. New technologies – atomic clocks, radar and laser ranging, space probes, cryogenic capabilities, to mention only a few – played a central role in this golden era. The period began with an experiment to confirm the gravitational frequency shift of light (1960) and ended with the reported decrease in the orbital period of the Hulse-Taylor binary pulsar at a rate consistent with the general relativistic prediction of gravitational-wave energy loss (1979). The results all supported general relativity, and most alternative theories of gravity fell by the wayside (for a popular review, see [1]).

Since that time, the field has entered what might be termed a Quest for Strong Gravity. Much like modern art, the term “strong” means different things to different people. To one steeped in general relativity, the principal figure of merit that distinguishes strong from weak gravity is the quantity  $\epsilon \sim GM/Rc^2$ , where  $G$  is the Newtonian gravitational constant,  $M$  is the characteristic mass scale of the phenomenon,  $R$  is the characteristic distance scale, and  $c$  is the speed of light. Near the event horizon of a non-rotating black hole, or for the expanding observable universe,  $\epsilon \sim 1$ ; for neutron stars,  $\epsilon \sim 0.2$ . These are the regimes of strong gravity. For the solar system,  $\epsilon < 10^{-5}$ ; this is the regime of weak gravity.

An alternative view of “strong” gravity comes from the world of particle physics. Here the figure of merit is  $GM/R^3c^2 \sim \ell^{-2}$ , where the Riemann curvature of spacetime associated with the phenomenon, represented by the left-hand-side, is comparable to the inverse square of a favorite length scale  $\ell$ . If  $\ell$  is the Planck length, this would correspond to the regime where one expects conventional quantum gravity effects to come into play. Another possible scale for  $\ell$  is the TeV scale associated with many models for unification of the forces, or models with extra spacetime dimensions. From this viewpoint, strong gravity is where the curvature is comparable to the inverse length squared. Weak gravity is where the curvature is much smaller than this. The universe at the Planck time is strong gravity. Just outside the event horizon of an astrophysical black hole is weak gravity.

Considerations of the possibilities for new physics from either point of view have led to a wide range of questions that will motivate new tests of general relativity as we move into its second century:

- Are the black holes that are in evidence throughout the universe truly the black holes of general relativity?
- Do gravitational waves propagate with the speed of light and do they contain more than the two basic polarization states of general relativity?
- Does general relativity hold on cosmological distance scales?
- Is Lorentz invariance strictly valid, or could it be violated at some detectable level?
- Does the principle of equivalence break down at some level?
- Are there testable effects arising from the quantization of gravity?

In this centenary assessment of the experimental basis of general relativity, we will summarize the current status of experiments, and attempt to chart the future of the subject. We will not provide complete references to early work done in this field but instead will refer the reader to selected recent papers and to the appropriate review articles and monographs. For derivations of many of the effects discussed in this article we will refer to *Theory and Experiment in Gravitational Physics* [2], hereafter referred to as TEGP; references to TEGP will be by chapter or section, e.g., “TEGP 8.9”. For a more comprehensive review, we refer readers to the author’s “Living Review” [3] (or its recent update [4])<sup>1</sup>. The “Resource Letter” by the author [5], contains 100 key references for experimental gravity.

## II. THE FOUNDATIONS OF GRAVITATION THEORY

### A. The Einstein equivalence principle

The principle of equivalence has historically played an important role in the development of gravitation theory. Newton regarded this principle as such a cornerstone of mechanics that he devoted the opening paragraph of the *Principia* to it. In 1907, Einstein used the principle as a basic element in his development of general relativity. We now regard the principle of equivalence as the foundation, not of Newtonian gravity or of general relativity, but of the broader idea that spacetime is curved. Much of this viewpoint can be traced back to Robert Dicke, who contributed crucial ideas about the foundations of gravitation theory between 1960 and 1965. These ideas were summarized in his influential Les Houches lectures of 1964 [6], and resulted in what has come to be called the Einstein equivalence principle (EEP).

One elementary equivalence principle is the kind Newton had in mind when he stated that the property of a body called “mass” is proportional to the “weight”, and is known as the weak equivalence principle (WEP). An alternative statement of WEP is that the trajectory of a freely falling “test” body (one not acted upon by such forces as electromagnetism, too small to be affected by tidal gravitational forces, and spinless) is independent of its internal structure and composition. In the simplest case of dropping two different bodies in a gravitational field, WEP states that the bodies fall with the same acceleration. This is often termed the Universality of Free Fall, or UFF.

The Einstein equivalence principle (EEP) is a more powerful and far-reaching concept; it has three components:

1. *Weak Equivalence Principle.* The trajectory of a freely falling “test” body is independent of its internal structure and composition.
2. *Local Lorentz Invariance.* The outcome of any local non-gravitational experiment is independent of the velocity of the freely-falling reference frame in which it is performed.
3. *Local Position Invariance.* The outcome of any local non-gravitational experiment is independent of where and when in the universe it is performed.

The Einstein equivalence principle is the heart and soul of gravitational theory, for it is possible to argue convincingly that if EEP is valid, then gravitation must be a “curved spacetime” phenomenon, in other words, gravity must be governed by a “metric theory of gravity”, whose postulates are:

---

<sup>1</sup> This article was prepared roughly in parallel with the author’s Living Review update, and may be considered a streamlined version of the latter. This will account for essentially identical prose between the two papers in numerous places

1. Spacetime is endowed with a symmetric metric.
2. The trajectories of freely falling test bodies are geodesics of that metric.
3. In local freely falling reference frames, the non-gravitational laws of physics are those written in the language of special relativity.

General relativity is a metric theory of gravity, but then so are many others, including the Brans–Dicke theory and its generalizations. It is not uncommon for modern variants of general relativity, especially those motivated by quantum gravity, unification, or extra dimensions, to introduce weak, *effective* violations of the metric postulates. Accordingly, it is important to test the various aspects of the Einstein equivalence principle thoroughly. We first survey the experimental tests, and describe some of the theoretical formalisms that have been developed to interpret them.

### 1. Tests of the weak equivalence principle

A direct test of WEP is the comparison of the acceleration of two laboratory-sized bodies of different composition in an external gravitational field. If the principle were violated, then the accelerations of different bodies would differ. A measurement or limit on the fractional difference in acceleration between two bodies then yields a quantity called the “Eötvös ratio” given by  $\eta \equiv 2|a_1 - a_2|/|a_1 + a_2|$ .

Many high-precision Eötvös-type experiments have been performed, from the pendulum experiments of Newton, Bessel, and Potter to the classic torsion-balance measurements of Eötvös, Dicke, Braginsky, and their collaborators. In modern torsion-balance experiments, two objects of different composition are connected by a rod or placed on a tray and suspended in a horizontal orientation by a fine wire. If the gravitational acceleration of the bodies differs, and this difference has a component perpendicular to the suspension wire, there will be a torque induced on the wire, related to the angle between the wire and the direction of the gravitational acceleration. Beginning in the late 1980s, numerous experiments were carried out primarily to search for a “fifth force”, but their null results also constituted tests of WEP. The “Eöt-Wash” experiments carried out at the University of Washington used a sophisticated torsion balance tray to compare the accelerations of various materials toward local topography on Earth, movable laboratory masses, the Sun and the galaxy, and have reached levels of  $2 \times 10^{-13}$  [7].

The recent development of atom interferometry has yielded tests of WEP, albeit to modest accuracy, comparable to that of the original Eötvös experiment. In these experiments, one measures the local acceleration of the two separated wavefunctions of an atom such as Cesium by studying the the interference pattern when the wavefunctions are combined, and compares that with the acceleration of a nearby macroscopic object of different composition [8, 9]. A claim [9] that these experiments test the gravitational redshift was subsequently shown to be incorrect [10]. Further improvements are anticipated [11].

The resulting upper limits on  $\eta$  are summarized in Figure 1 (for an extensive bibliography of experiments up to 1991, see [12]).

A number of projects are in the development or planning stage to push the bounds on  $\eta$  even lower. The project MICROSCOPE is designed to test WEP to  $10^{-15}$ . It is being developed by the French space agency CNES for launch in late 2015, for a one-year mission. The drag-compensated satellite will be in a Sun-synchronous polar orbit at 700 km altitude, with a payload consisting of two differential accelerometers, one with elements made of the same material (platinum), and another with elements made of different materials (platinum and titanium). Other concepts for future improvements include advanced space experiments (Galileo-Galilei, STEP), lunar laser ranging (see Sec. VC1), binary pulsar observations, and experiments with anti-hydrogen. For a review of past and future tests of WEP, see Vol. 29, Issue 18 of *Classical and Quantum Gravity* [13] and the review by Adelberger et al. [14].

### 2. Tests of local Lorentz invariance

Although special relativity itself never benefited from the kind of “crucial” experiments, such as the perihelion advance of Mercury and the deflection of light, that contributed so much to the initial acceptance of general relativity and to the fame of Einstein, the steady accumulation of experimental support, together with the successful merger of special relativity with quantum mechanics, led to its being accepted by mainstream physicists by the late 1920s, ultimately to become part of the standard toolkit of every working physicist. This accumulation included

- the classic Michelson–Morley experiment and its descendents;
- the Ives–Stillwell, Rossi–Hall, and other tests of time-dilation;

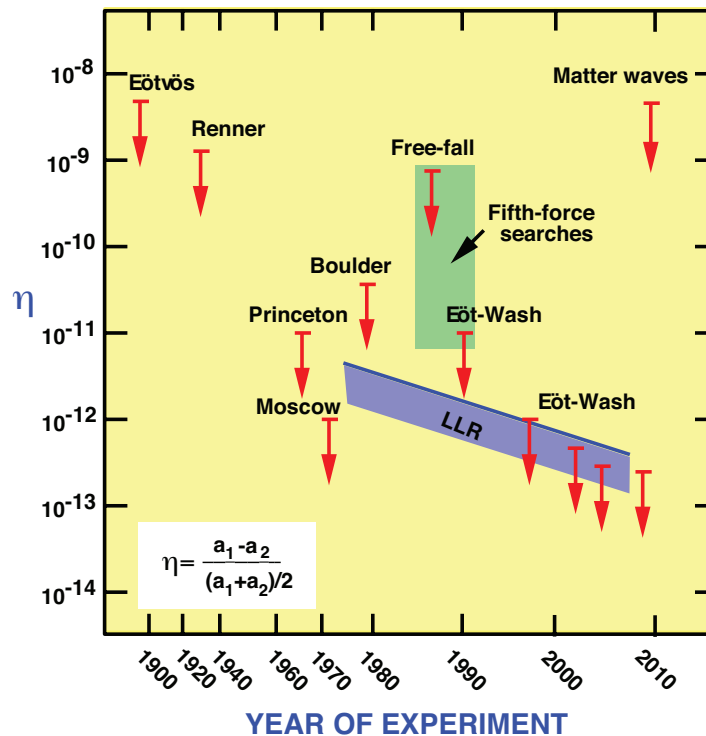


FIG. 1: Selected tests of the weak equivalence principle, showing bounds on  $\eta$ . The free-fall and Eöt-Wash experiments were originally performed to search for a fifth force (green region, representing many experiments). The blue band shows evolving bounds on  $\eta$  for gravitating bodies from lunar laser ranging (LLR).

- tests of the independence of the speed of light of the velocity of the source, using both binary X-ray stellar sources and high-energy pions;
- tests of the isotropy of the speed of light.

In addition to these direct experiments, there was the Dirac equation of quantum mechanics and its prediction of anti-particles and spin; later would come the stunningly successful relativistic theory of quantum electrodynamics. For a pedagogical review on the occasion of the 2005 centenary of special relativity, see [15].

In 2015, on the 110th anniversary of special relativity, one might ask “what is there left to test?” Special relativity has been so thoroughly integrated into the fabric of modern physics that its validity is rarely challenged, except by cranks and crackpots. It is ironic then, that during the past 15 years, a vigorous theoretical and experimental effort has been launched to find violations of special relativity. The motivation for this effort is not a desire to repudiate Einstein, but to look for evidence of new physics “beyond” Einstein, such as apparent, or “effective” violations of Lorentz invariance that might result from certain models of quantum gravity. Quantum gravity asserts that there is a fundamental length scale given by the Planck length,  $\ell_{\text{Pl}} = (\hbar G/c^3)^{1/2} = 1.6 \times 10^{-33}$  cm, but since length is not an invariant quantity (Lorentz–FitzGerald contraction), then there could be a violation of Lorentz invariance at some level in quantum gravity. In brane world scenarios, while physics may be locally Lorentz invariant in the higher dimensional world, the confinement of the interactions of normal physics to our four-dimensional “brane” could induce apparent Lorentz violating effects. And in models such as string theory, the presence of additional vector and tensor long-range fields that couple to matter of the standard model could induce effective violations of Lorentz symmetry. These and other ideas have motivated a serious reconsideration of how to test Lorentz invariance with better precision and in new ways.

A simple and useful way of interpreting some of these modern experiments, called the  $c^2$ -formalism, is to suppose that the electromagnetic interactions suffer a slight violation of Lorentz invariance, through a change in the speed of electromagnetic radiation  $c$  relative to the limiting speed of material test particles ( $c_0$ , made to take the value unity via a choice of units), in other words,  $c \neq 1$ . Such a violation necessarily selects a preferred universal rest frame, presumably that of the cosmic background radiation, through which we are moving at about  $370 \text{ km s}^{-1}$ . Such a Lorentz-non-invariant electromagnetic interaction would cause shifts in the energy levels of atoms and nuclei that depend on the orientation of the quantization axis of the state relative to our universal velocity vector, and on the

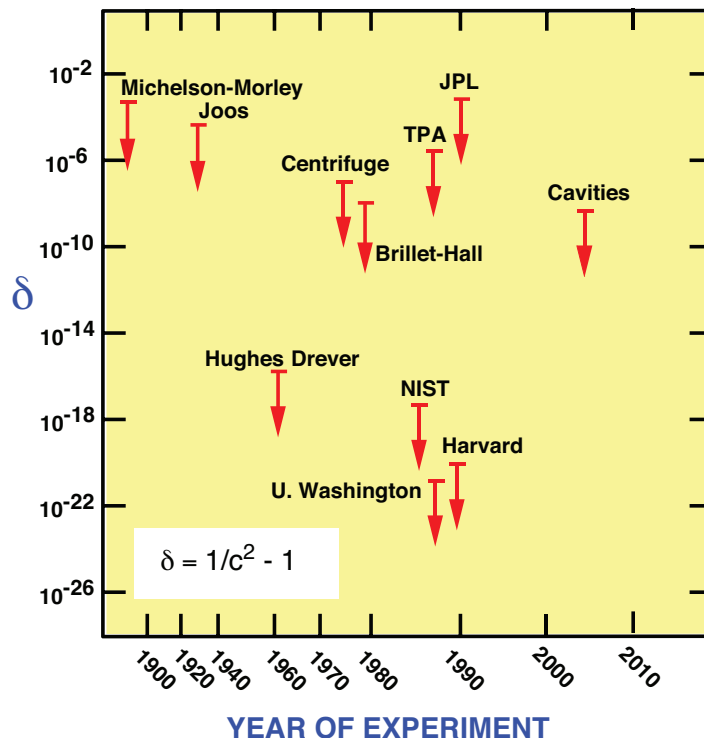


FIG. 2: Selected tests of local Lorentz invariance showing the bounds on the parameter  $\delta$ , which measures the degree of violation of Lorentz invariance in electromagnetism. The Michelson–Morley, Joos, Brillet–Hall and cavity experiments test the isotropy of the round-trip speed of light. The centrifuge, two-photon absorption (TPA) and JPL experiments test the isotropy of light speed using one-way propagation. The most precise experiments test isotropy of atomic energy levels.

quantum numbers of the state. The presence or absence of such energy shifts can be examined by measuring the energy of one such state relative to another state that is either unaffected or is affected differently by the supposed violation. The magnitude of these “clock anisotropies” turn out to be proportional to  $\delta \equiv |c^{-2} - 1|$  (see TEGP 2.6(a) for details).

The earliest clock anisotropy experiments were the Hughes–Drever experiments, performed in the period 1959–60, yielding limits on the parameter  $\delta$  shown in Fig. 2. Dramatic improvements were made in the 1980s using laser-cooled trapped atoms and ions, which made it possible to reduce the broadening of resonance lines caused by collisions. Also included for comparison in Fig. 2 is the corresponding limit obtained from Michelson–Morley type experiments and their modern variants such as the Brillet–Hall experiment, and comparisons between cavity oscillators and atomic clocks.

The  $c^2$  framework focusses exclusively on classical electrodynamics. It has been extended to the entire standard model of particle physics by Kostelecký and collaborators. Called the Standard Model Extension (SME), it takes the standard  $SU(3) \times SU(2) \times U(1)$  field theory of particle physics, and modifies the terms in the action by inserting a variety of tensorial quantities in the quark, lepton, Higgs, and gauge boson sectors that could explicitly violate LLI. The modified terms split naturally into those that are odd under CPT (i.e. that violate CPT) and terms that are even under CPT. The result is a rich and complex framework, with many parameters to be analyzed and tested by experiment. Experimentalists have risen to the challenge, and have placed interesting bounds on many of the SME parameters. A variety of clock anisotropy experiments have been carried out to bound the electromagnetic parameters of the SME framework. Other testable effects of Lorentz-invariance violation include arrival-time variations in TeV gamma-ray bursts from blazars, threshold effects in particle reactions, birefringence in photon propagation, gravitational Cerenkov radiation, and neutrino oscillations. The details of the SME and other approaches to testing LLI are beyond the scope of this article; the reader is referred to the reviews by Mattingly [16], Liberati [17] and Kostelecký and Russell [18]. The last article gives “data tables” showing experimental bounds on all the various parameters of the model. The SME has also been extended to a parametrization of local Lorentz violations in gravity (see, for example, [19]).

### 3. Tests of local position invariance

The principle of local position invariance, the third part of EEP, can be tested by the gravitational redshift experiment, the first experimental test of gravitation proposed by Einstein, eight years before the full theory of general relativity. Despite the fact that Einstein regarded this as a crucial test of general relativity, we now realize that it does not distinguish between general relativity and any other metric theory of gravity, but is only a test of EEP. A typical gravitational redshift experiment measures the frequency or wavelength shift  $Z \equiv \Delta\nu/\nu = -\Delta\lambda/\lambda = \Delta U/c^2$  between two identical frequency standards (clocks) placed at rest at different heights in a static gravitational potential  $U$ . If LPI is not valid, then it turns out that the shift can be written

$$Z = (1 + \alpha) \frac{\Delta U}{c^2}, \quad (1)$$

where the parameter  $\alpha$  may depend upon the nature of the clock whose shift is being measured (see TEGP 2.4 (c) for details).

The first successful, high-precision redshift measurement was the series of Pound–Rebka–Snider experiments of 1960–1965 that measured the frequency shift of gamma-ray photons from  $^{57}\text{Fe}$  as they ascended or descended the Jefferson Physical Laboratory tower at Harvard University. The high accuracy achieved – one percent – was obtained by making use of the Mössbauer effect to produce a narrow resonance line whose shift could be accurately determined. Other experiments since 1960 measured the shift of spectral lines in the Sun’s gravitational field and the change in rate of atomic clocks transported aloft on aircraft, rockets and satellites. Figure 3 summarizes the important test of LPI that have been performed since 1960.

After almost 50 years of inconclusive or contradictory measurements, the gravitational redshift of solar spectral lines was finally measured reliably. During the early years of general relativity, the failure to measure this effect in solar lines was seized upon by some as reason to doubt the theory. Unfortunately, the measurement is not simple. Solar spectral lines are subject to the “limb effect”, a variation of line wavelengths between the center of the solar disk and its edge or “limb”; this effect is actually a Doppler shift caused by complex convective and turbulent motions in the photosphere and lower chromosphere, and is expected to be minimized by observing at the solar limb, where the motions are predominantly transverse. The secret is to use strong, symmetrical lines, leading to unambiguous wavelength measurements. Successful measurements were finally made in 1962 and 1972. In 1991, LoPresto et al. measured the solar shift in agreement with LPI to about 2 percent by observing the oxygen triplet lines both in absorption in the limb and in emission just off the limb [20].

The most precise standard redshift test to date was the Vessot–Levine rocket experiment known as Gravity Probe-A (GPA) that took place in June 1976. A hydrogen-maser clock was flown on a rocket to an altitude of about 10,000 km and its frequency compared to a similar clock on the ground. Analysis of the data yielded a limit  $|\alpha| < 2 \times 10^{-4}$ .

A “null” redshift experiment performed in 1978 tested whether the *relative* rates of two different clocks — hydrogen masers and cavity stabilized oscillators — depended upon the diurnal and annual variations of the solar gravitational potential at the location of the laboratory. This bound was subsequently improved using more stable frequency standards, such as atomic fountain clocks. The best current bounds, from comparing various pairings of Rubidium, Cesium, Hydrogen and isotopes of Dysprosium [21–23] hover around the one part per million mark.

The Atomic Clock Ensemble in Space (ACES) project will place both a cold trapped atom clock based on Cesium called PHARAO (Projet d’Horloge Atomique par Refroidissement d’Atomes en Orbit), and an advanced hydrogen maser clock on the International Space Station to measure the gravitational redshift to parts in  $10^6$ , as well as to carry out a number of fundamental physics experiments and to enable improvements in global timekeeping. Launch is currently scheduled for May 2016.

Modern navigation using Earth-orbiting atomic clocks and accurate time-transfer must routinely take gravitational redshift and time-dilation effects into account. For example, the Global Positioning System (GPS) provides absolute positional accuracies of around 15 m (even better in its military mode), and 50 nanoseconds in time transfer accuracy, anywhere on Earth. Yet the difference in rate between satellite and ground clocks as a result of relativistic effects is a whopping 39 *microseconds* per day (46  $\mu\text{s}$  from the gravitational redshift, and  $-7 \mu\text{s}$  from time dilation). If these effects were not accurately accounted for, GPS would fail to function at its stated accuracy. This represents a welcome practical application of general relativity! For the role of general relativity in GPS, see [24]; for a popular essay, see [25].

Local position invariance also refers to position in time. If LPI is satisfied, the fundamental constants of non-gravitational physics should be constants in time. Table I shows current bounds on cosmological variations in selected dimensionless constants. For discussion and references to early work, see TEGP 2.4 (c) or [26]. For a comprehensive recent review both of experiments and of theoretical ideas that underly proposals for varying constants, see [27].

Experimental bounds on varying constants come in two types: bounds on the present rate of variation, and bounds on the difference between today’s value and a value in the distant past. The main example of the former type is

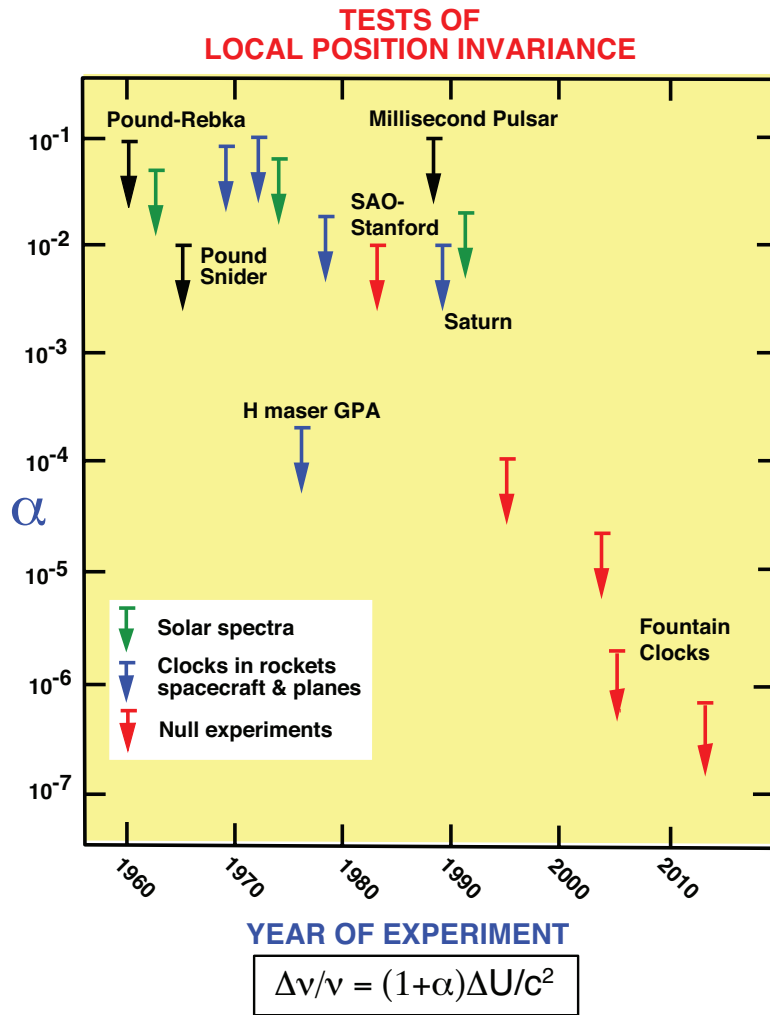


FIG. 3: Selected tests of local position invariance via gravitational redshift experiments, showing bounds on  $\alpha$ , which measures degree of deviation of redshift from the formula  $\Delta\nu/\nu = \Delta U/c^2$ . In null redshift experiments, the bound is on the difference in  $\alpha$  between different kinds of clocks.

the clock comparison test, in which highly stable atomic clocks of different fundamental type are intercompared over periods ranging from months to years (variants of the null redshift experiment). The second type of bound involves measuring the relics of or signal from a process that occurred in the distant past and comparing the inferred value of the constant with the value measured in the laboratory today. One sub-type uses astronomical measurements of spectral lines at large redshift, while the other uses fossils of nuclear processes on Earth to infer values of constants early in geological history, notably from the Oklo natural nuclear reactor in Gabon. Despite continuing reports by one group [28] of a variation of the fine structure constant over cosmic time as seen in spectral lines, most groups find no significant variation (eg. [29, 30]).

#### 4. *EEP, particle physics, and the search for new interactions*

There is mounting theoretical evidence to suggest that EEP is likely to be violated at some level, whether by quantum gravity effects, by effects arising from string theory, or by hitherto undetected interactions. As a result, EEP and related tests are now viewed as ways to discover or place constraints on new physical interactions, or as a branch of “non-accelerator particle physics”, searching for the possible imprints of high-energy particle effects in the low-energy realm of gravity. One example of this is the “fifth-force” episode of the middle 1980s, in which Eötvös-type experiments and tests of the gravitational inverse-square law were used to limit the existence of intermediate-range forces that could arise from particle interactions beyond the standard model. Tests of the inverse square law at

TABLE I: Bounds on cosmological variation of fundamental constants of non-gravitational physics. For an in-depth review, see [27].

Constant $k$	Limit on $\dot{k}/k$ Redshift ( $\text{yr}^{-1}$ )	Method
Fine structure constant ( $\alpha_{\text{EM}} = e^2/\hbar c$ )	$1.3 \times 10^{-16}$ 0	Clock comparisons
	$0.5 \times 10^{-16}$ 0.15	Oklo Natural Reactor
	$3.4 \times 10^{-16}$ 0.45	$^{187}\text{Re}$ decay in meteorites
	$1.2 \times 10^{-16}$ 0.4–2.3	Spectra in distant quasars
Weak interaction constant ( $\alpha_{\text{W}} = G_{\text{f}}m_{\text{p}}^2c/\hbar^3$ )	$1 \times 10^{-11}$ 0.15	Oklo Natural Reactor
	$5 \times 10^{-12}$ $10^9$	Big Bang nucleosynthesis
e-p mass ratio	$3.3 \times 10^{-15}$ 0	Clock comparisons
	$3 \times 10^{-15}$ 2.6–3.0	Spectra in distant quasars

sub-mm distance scales continue in an effort to search for evidence of extra dimensions or light scalar particles [14]. Anomalies in the orbit of the Pioneer 10 and 11 spacecraft at 20 to 70 astronomical units from the Sun were touted for a time as evidence for new physics, but were ultimately shown to be the result of anisotropic emission of heat from the spacecraft [31, 32].

## B. Metric theories of gravity and the strong equivalence principle

The Einstein equivalence principle is strongly supported by empirical evidence, as we have seen. This tells us that the only theories of gravity that have a hope of being viable are metric theories, or possibly theories that at worst admit very weak or short-range non-metric couplings. Therefore for the remainder of this article, we will turn our attention exclusively to metric theories of gravity.

The property that all non-gravitational fields should couple in the same manner to a single gravitational field is sometimes called “universal coupling”. Because of it, one can discuss the metric as a property of spacetime itself rather than as a field over spacetime. This is because its properties may be measured and studied using a variety of different experimental devices, composed of different non-gravitational fields and particles, and, because of universal coupling, the results will be independent of the device. Thus, for instance, the proper time between two events is a characteristic of spacetime and of the location of the events, not of the clocks used to measure it.

Mathematically, if EEP is valid, the non-gravitational laws of physics may be formulated by taking their special relativistic forms in terms of the Minkowski metric  $\eta$  and simply “going over” to new forms in terms of the curved spacetime metric  $g$ , using the mathematics of differential geometry. The details of this “going over” can be found in standard textbooks (see [33], TEGP 3.2.).

In any metric theory of gravity, matter and non-gravitational fields respond only to the spacetime metric  $g$ . In principle, however, there could exist other gravitational fields besides the metric, such as scalar fields, vector fields, and so on. The role of such fields is to mediate the manner in which matter and non-gravitational fields generate gravitational fields and produce the metric; once determined, however, the metric alone acts back on the matter in the manner prescribed by EEP.

What distinguishes one metric theory from another, therefore, is the number and kind of gravitational fields it contains in addition to the metric, and the equations that determine the structure and evolution of these fields. The fields could be dynamical, in that they obey their own set of dynamical equations, or they could be “fixed” or non-dynamical — an example of the latter is a background Minkowski metric.

General relativity is a purely dynamical theory since it contains only one gravitational field, the metric itself, and its structure and evolution are governed by partial differential equations (Einstein’s equations). Brans–Dicke theory and its generalizations are purely dynamical theories; the field equation for the metric involves the scalar field (as well as the matter as source), and that for the scalar field involves the metric.

Consider now a local gravitating system, as described by a chosen metric theory. The system could be a star, a black hole, the solar system, or a Cavendish experiment. Because the metric is coupled directly or indirectly to the other fields of the theory, the gravitational environment in which the local gravitating system resides can influence the metric generated by the local system via the boundary values of the auxiliary fields. Those boundary values typically depend on the distribution of matter external to the system. Consequently, the results of local gravitational experiments



may depend on the location and velocity of the frame relative to the external environment. Of course, local *non*-gravitational experiments are unaffected since the gravitational fields they generate are assumed to be negligible, and since those experiments couple only to the metric, whose form can always be made locally Minkowskian at a given spacetime event.

A theory which contains only the metric  $\mathbf{g}$  (such as general relativity) yields local gravitational physics which is independent of the location and velocity of the local system. This follows from the fact that the only field coupling the local system to the environment is  $\mathbf{g}$ , and it is always possible to find a coordinate system in which  $\mathbf{g}$  takes the Minkowski form at the boundary between the local system and the external environment (neglecting inhomogeneities in the external gravitational field). Thus, apart from standard tidal effects, the external environment cannot act back on the local gravitating system.

A theory which contains the metric  $\mathbf{g}$  and dynamical scalar fields  $\varphi_A$  yields local gravitational physics which may depend on the location of the frame but which is independent of the velocity of the frame. This follows from the asymptotic Lorentz invariance of the Minkowski metric and of the scalar fields, but now the asymptotic values of the scalar fields may depend on the location of the frame. For example in scalar-tensor theories, the effective gravitational coupling strength depends on the scalar field, which may vary in space and time, depending on the external environment.

A theory which contains the metric  $\mathbf{g}$  and additional dynamical vector or tensor fields or prior-geometric fields yields local gravitational physics which may have both location and velocity-dependent effects. These ideas can be summarized in the strong equivalence principle (SEP), which states that:

1. WEP is valid for self-gravitating bodies as well as for test bodies.
2. The outcome of any local test experiment is independent of the velocity of the (freely falling) apparatus.
3. The outcome of any local test experiment is independent of where and when in the universe it is performed.

The distinction between SEP and EEP is the inclusion of bodies with self-gravitational interactions (planets, stars) and of experiments involving gravitational forces (Cavendish experiments, gravimeter measurements). Note that SEP contains EEP as the special case in which local gravitational forces are ignored.

General relativity seems to be the only viable metric theory that embodies SEP completely. In Section V C, we will discuss experimental evidence for the validity of SEP.

### III. THE PARAMETRIZED POST-NEWTONIAN FORMALISM

Despite the possible existence of long-range gravitational fields in addition to the metric, matter and non-gravitational fields are completely oblivious to them in metric theories of gravity. The only gravitational field that enters the equations of motion is the metric  $\mathbf{g}$ . Thus the metric and the equations of motion for matter become the primary entities for calculating observable effects, and all that distinguishes one metric theory from another is the particular way in which matter and possibly other gravitational fields generate the metric.

The comparison of metric theories of gravity with each other and with experiment becomes particularly simple when one takes the slow-motion, weak-field limit. This approximation, known as the post-Newtonian limit, is sufficiently accurate to encompass most solar-system tests that can be performed in the foreseeable future. In this limit, the spacetime metric  $\mathbf{g}$  predicted by a broad class of metric theories of gravity has the same structure. It can be written as an expansion about the Minkowski metric ( $\eta_{\mu\nu} = \text{diag}(-1, 1, 1, 1)$ ) in terms of dimensionless gravitational potentials of varying degrees of smallness. These potentials are constructed from the matter variables, such as mass density  $\rho$ , energy density  $\rho\Pi$ , pressure  $p$ , four-velocity  $u^\alpha$ , ordinary velocity  $v^j \equiv u^j/u^0$ , etc., in imitation of the Newtonian gravitational potential

$$U(\mathbf{x}, t) \equiv G \int \rho(\mathbf{x}', t) |\mathbf{x} - \mathbf{x}'|^{-1} d^3x'. \quad (2)$$

The “order of smallness” is determined according to the rules  $U/c^2 \sim (v/c)^2 \sim \Pi/c^2 \sim p/\rho c^2 \sim \epsilon$ ,  $v^i/c \sim |d/d(ct)|/|d/dx| \sim \epsilon^{1/2}$ , and so on.

A consistent post-Newtonian limit requires determination of  $g_{00}$  correct through  $\mathcal{O}(\epsilon^2)$ ,  $g_{0i}$  through  $\mathcal{O}(\epsilon^{3/2})$ , and  $g_{ij}$  through  $\mathcal{O}(\epsilon)$  (for details see TEGP 4.1 or [34]). The only way that one metric theory differs from another is in the numerical values of the coefficients that appear in front of the metric potentials. The parametrized post-Newtonian (PPN) formalism inserts parameters in place of these coefficients, parameters whose values depend on the theory under study. In the current version of the PPN formalism, ten parameters are used, chosen in such a manner that they measure or indicate general properties of metric theories of gravity (see Table II). Under reasonable assumptions

TABLE II: The PPN Parameters and their significance (note that  $\alpha_3$  has been shown twice to indicate that it is a measure of two effects).

Parameter and what it measures relative to GR	Value in GR	Value in semi-conservative theories	Value in fully conservative theories
$\gamma$   How much space-curvature produced by unit rest mass?	1	$\gamma$	$\gamma$
$\beta$   How much “nonlinearity” in the superposition law for gravity?	1	$\beta$	$\beta$
$\xi$   Preferred-location effects?	0	$\xi$	$\xi$
$\alpha_1$   Preferred-frame effects?	0	$\alpha_1$	0
$\alpha_2$	0	$\alpha_2$	0
$\alpha_3$	0	0	0
$\alpha_3$   Violation of conservation of total momentum?	0	0	0
$\zeta_1$	0	0	0
$\zeta_2$	0	0	0
$\zeta_3$	0	0	0
$\zeta_4$	0	0	0

about the kinds of potentials that can be present at post-Newtonian order (basically only Poisson-like potentials), one finds that ten PPN parameters exhaust the possibilities.

The parameters  $\gamma$  and  $\beta$  are the usual Eddington–Robertson–Schiff parameters used to describe the “classical” tests of general relativity, and are in some sense the most important; they are the only non-zero parameters in general relativity and scalar-tensor gravity. The parameter  $\xi$  is non-zero in a class of theories of gravity that predict preferred-location effects such as a galaxy-induced anisotropy in the local gravitational constant  $G_L$  (also called “Whitehead” effects);  $\alpha_1$ ,  $\alpha_2$ ,  $\alpha_3$  measure whether or not the theory predicts post-Newtonian preferred-frame effects;  $\alpha_3$ ,  $\zeta_1$ ,  $\zeta_2$ ,  $\zeta_3$ ,  $\zeta_4$  measure whether or not the theory predicts violations of global conservation laws for total momentum. In Table II we show the values these parameters take in general relativity; in any theory of gravity that possesses conservation laws for total momentum, called “semi-conservative” (any theory that is based on an invariant action principle is semi-conservative); and in any theory that in addition possesses six global conservation laws for angular momentum, called “fully conservative” (such theories automatically predict no post-Newtonian preferred-frame effects). Semi-conservative theories have five free PPN parameters ( $\gamma$ ,  $\beta$ ,  $\xi$ ,  $\alpha_1$ ,  $\alpha_2$ ) while fully conservative theories have three ( $\gamma$ ,  $\beta$ ,  $\xi$ ).

The PPN formalism was pioneered by Kenneth Nordtvedt [35], who studied the post-Newtonian metric of a system of gravitating point masses, extending earlier work by Eddington, Robertson and Schiff (TEGP 4.2). Will [36] generalized the framework to perfect fluids. A general and unified version of the PPN formalism was developed by Will and Nordtvedt [37]. The canonical version, with conventions altered to be more in accord with standard textbooks such as [38], is discussed in detail in TEGP, Chapter 4.

#### IV. COMPETING THEORIES OF GRAVITY

One of the important applications of the PPN formalism is the comparison and classification of alternative metric theories of gravity. The population of viable theories has fluctuated over the years as new effects and tests have been discovered, largely through the use of the PPN framework, which eliminated many theories thought previously to be viable. The theory population has also fluctuated as new, potentially viable theories have been invented.

In this review, we will focus on general relativity, the general class of scalar-tensor modifications of it, of which the Jordan–Fierz–Brans–Dicke theory (Brans–Dicke, for short) is the classic example, and vector-tensor or scalar-vector-tensor theories. The reasons are several-fold:

- A full compendium of alternative theories circa 1981 is given in TEGP, Chapter 5.
- Many alternative metric theories developed during the 1970s and 1980s could be viewed as “straw-man” theories, invented to prove that such theories exist or to illustrate particular properties. Few of these could be regarded

as well-motivated theories from the point of view, say, of field theory or particle physics.

- A number of theories fall into the class of “prior-geometric” theories, with absolute elements such as a flat background metric in addition to the physical metric. Most of these theories predict “preferred-frame” effects, that have been tightly constrained by observations (see Section V C 2). An example is Rosen’s bimetric theory.
- A large number of alternative theories of gravity predict gravitational wave emission substantially different from that of general relativity, in strong disagreement with observations of the binary pulsar (see Section VIII).
- Scalar-tensor modifications of general relativity have become very popular in unification schemes such as string theory, and in cosmological model building. Because the scalar fields could be massive, the potentials in the post-Newtonian limit could be modified by Yukawa-like terms.
- Theories that also incorporate vector fields have attracted recent attention, in the spirit of the SME (see Section II A 2), as models for violations of Lorentz invariance in the gravitational sector, and as potential candidates to account for phenomena such as galaxy rotation curves without resorting to dark matter.

### A. General relativity

The metric  $\mathbf{g}$  is the sole dynamical field, and the theory contains no arbitrary functions or parameters, apart from the value of the Newtonian coupling constant  $G$ , which is measurable in laboratory experiments. Throughout this article, we ignore the cosmological constant  $\Lambda_C$ . We do this despite recent evidence, from supernova data, of an accelerating universe, which would indicate either a non-zero cosmological constant or a dynamical “dark energy” contributing about 70 percent of the critical density. Although  $\Lambda_C$  has significance for quantum field theory, quantum gravity, and cosmology, on the scale of the solar-system or of stellar systems its effects are negligible, for the values of  $\Lambda_C$  inferred from supernova observations. On the other hand, the conundrum of accelerated expansion has motivated the development of alternative theories of gravity, notably of the so-called  $f(R)$  type.

The field equations of general relativity are derivable from an invariant action principle  $\delta I = 0$ , where

$$I = \frac{c^3}{16\pi G} \int R(-g)^{1/2} d^4x + I_m(\psi_m, g_{\mu\nu}), \quad (3)$$

where  $R$  is the Ricci scalar, and  $I_m$  is the matter action, which depends on matter fields  $\psi_m$  universally coupled to the metric  $\mathbf{g}$ . By varying the action with respect to  $g_{\mu\nu}$ , we obtain the field equations

$$G_{\mu\nu} \equiv R_{\mu\nu} - \frac{1}{2}g_{\mu\nu}R = \frac{8\pi G}{c^4}T_{\mu\nu}, \quad (4)$$

where  $T_{\mu\nu}$  is the matter energy-momentum tensor. General covariance of the matter action implies the equations of motion  $T^{\mu\nu}{}_{;\nu} = 0$ ; varying  $I_m$  with respect to  $\psi_m$  yields the matter field equations of the Standard Model. By virtue of the *absence* of prior-geometric elements, the equations of motion are also a consequence of the field equations via the Bianchi identities  $G^{\mu\nu}{}_{;\nu} = 0$ .

The general procedure for deriving the post-Newtonian limit of metric theories is spelled out in TEGP 5.1, and is described in detail for general relativity in TEGP 5.2, or Chapter 8 of [34]. The PPN parameter values are listed in Table III.

### B. Scalar-tensor theories

These theories contain the metric  $\mathbf{g}$ , a scalar field  $\varphi$ , a potential function  $V(\varphi)$ , and a coupling function  $A(\varphi)$  (generalizations to more than one scalar field have also been carried out [39]). For some purposes, the action is conveniently written in a non-metric representation, sometimes denoted the “Einstein frame”, in which the gravitational action looks exactly like that of general relativity:

$$\begin{aligned} \tilde{I} = & \frac{c^3}{16\pi G} \int \left[ \tilde{R} - 2\tilde{g}^{\mu\nu} \partial_\mu \varphi \partial_\nu \varphi - V(\varphi) \right] (-\tilde{g})^{1/2} d^4x \\ & + I_m(\psi_m, A^2(\varphi)\tilde{g}_{\mu\nu}), \end{aligned} \quad (5)$$

TABLE III: Metric theories and their PPN parameter values ( $\alpha_3 = \zeta_i = 0$  for all cases). The parameters  $\gamma'$ ,  $\beta'$ ,  $\alpha'_1$ , and  $\alpha'_2$  denote complicated functions of the arbitrary constants and matching parameters.

Theory	Arbitrary functions or constants	Cosmic matching parameters	PPN parameters				
			$\gamma$	$\beta$	$\xi$	$\alpha_1$	$\alpha_2$
General relativity	none	none	1	1	0	0	0
Scalar-tensor							
Brans–Dicke	$\omega_{\text{BD}}$	$\phi_0$	$\frac{1 + \omega_{\text{BD}}}{2 + \omega_{\text{BD}}}$	1	0	0	0
General, $f(R)$	$A(\varphi), V(\varphi)$	$\varphi_0$	$\frac{1 + \omega}{2 + \omega}$	$1 + \frac{\lambda}{4 + 2\omega}$	0	0	0
Vector-tensor							
Unconstrained	$\omega, c_1, c_2, c_3, c_4$	$u$	$\gamma'$	$\beta'$	0	$\alpha'_1$	$\alpha'_2$
Einstein-Æther	$c_1, c_2, c_3, c_4$	none	1	1	0	$\alpha'_1$	$\alpha'_2$
Khronometric	$\alpha_K, \beta_K, \lambda_K$	none	1	1	0	$\alpha'_1$	$\alpha'_2$
Tensor-Vector-Scalar	$k, c_1, c_2, c_3, c_4$	$\phi_0$	1	1	0	$\alpha'_1$	$\alpha'_2$

where  $\tilde{R} \equiv \tilde{g}^{\mu\nu} \tilde{R}_{\mu\nu}$  is the Ricci scalar of the ‘‘Einstein’’ metric  $\tilde{g}_{\mu\nu}$ . This representation is a ‘‘non-metric’’ one because the matter fields  $\psi_m$  couple to a combination of  $\varphi$  and  $\tilde{g}_{\mu\nu}$ . Despite appearances, however, it is a metric theory, because it can be put into a metric representation by identifying the ‘‘physical metric’’

$$g_{\mu\nu} \equiv A^2(\varphi) \tilde{g}_{\mu\nu}. \quad (6)$$

The action can then be rewritten in the metric form

$$I = \frac{c^3}{16\pi G} \int [\phi R - \phi^{-1} \omega(\phi) g^{\mu\nu} \partial_\mu \phi \partial_\nu \phi - \phi^2 V] (-g)^{1/2} d^4x + I_m(\psi_m, g_{\mu\nu}), \quad (7)$$

where

$$\begin{aligned} \phi &\equiv A(\varphi)^{-2}, \\ 3 + 2\omega(\phi) &\equiv \alpha(\varphi)^{-2}, \\ \alpha(\varphi) &\equiv \frac{d(\ln A(\varphi))}{d\varphi}. \end{aligned} \quad (8)$$

The Einstein frame is useful for discussing general characteristics of such theories, and for some cosmological applications, while the metric representation is most useful for calculating observable effects. The field equations, post-Newtonian limit and PPN parameters are discussed in TEGP 5.3, and the values of the PPN parameters are listed in Table III.

The parameters that enter the post-Newtonian limit are

$$\omega \equiv \omega(\phi_0), \quad \lambda \equiv \left[ \frac{\phi d\omega/d\phi}{(3 + 2\omega)(4 + 2\omega)} \right]_{\phi_0}, \quad (9)$$

where  $\phi_0$  is the value of  $\phi$  today far from the system being studied, as determined by appropriate cosmological boundary conditions. In Brans–Dicke theory ( $\omega(\phi) \equiv \omega_{\text{BD}} = \text{const.}$ ), the larger the value of  $\omega_{\text{BD}}$ , the smaller the effects of the scalar field, and in the limit  $\omega_{\text{BD}} \rightarrow \infty$  ( $\alpha_0 \rightarrow 0$ ), the theory becomes indistinguishable from general relativity in all its predictions. In more general theories, the function  $\omega(\phi)$  could have the property that, at the present epoch, and in weak-field situations, the value of the scalar field  $\phi_0$  is such that  $\omega$  is very large and  $\lambda$  is very small (theory almost identical to general relativity today), but that for past or future values of  $\phi$ , or in strong-field regions such as the interiors of neutron stars,  $\omega$  and  $\lambda$  could take on values that would lead to significant differences from general relativity.

Damour and Esposito-Farèse [39] have adopted an alternative parametrization of scalar-tensor theories, in which one expands  $\ln A(\varphi)$  about a cosmological background field value  $\varphi_0$ :

$$\ln A(\varphi) = \alpha_0(\varphi - \varphi_0) + \frac{1}{2}\beta_0(\varphi - \varphi_0)^2 + \dots \quad (10)$$

A precisely linear coupling function produces Brans–Dicke theory, with  $\alpha_0^2 = 1/(2\omega_{\text{BD}} + 3)$ , or  $1/(2 + \omega_{\text{BD}}) = 2\alpha_0^2/(1 + \alpha_0^2)$ . The function  $\ln A(\varphi)$  acts as a potential for the scalar field  $\varphi$  within matter, and, if  $\beta_0 > 0$ , then during cosmological evolution, the scalar field naturally evolves toward the minimum of the potential, i.e. toward  $\alpha_0 \approx 0$ ,  $\omega \rightarrow \infty$ , or toward a theory close to, though not precisely general relativity [40, 41]. Estimates of the expected relic deviations from general relativity today in such theories depend on the cosmological model, but range from  $10^{-5}$  to a few times  $10^{-7}$  for  $|\gamma - 1|$ .

Negative values of  $\beta_0$  correspond to a “locally unstable” scalar potential (the overall theory is still stable in the sense of having no tachyons or ghosts). In this case, objects such as neutron stars can experience a “spontaneous scalarization”, whereby the interior values of  $\varphi$  can take on values very different from the exterior values, through non-linear interactions between strong gravity and the scalar field, dramatically affecting the stars’ internal structure and leading to strong violations of SEP. On the other hand, in the case  $\beta_0 < 0$ , one must confront that fact that, with an unstable  $\varphi$  potential, cosmological evolution would presumably drive the system away from the peak where  $\alpha_0 \approx 0$ , toward parameter values that could be excluded by solar system experiments.

Scalar fields coupled to gravity or matter are also ubiquitous in particle-physics-inspired models of unification, such as string theory. In some models, the coupling to matter may lead to violations of EEP, which could be tested or bounded by the experiments described in Section II A. In many models the scalar field could be massive; if the Compton wavelength is of macroscopic scale, its effects are those of a “fifth force”. Only if the theory can be cast as a metric theory with a scalar field of infinite range or of range long compared to the scale of the system in question (solar system) can the PPN framework be strictly applied. If the mass of the scalar field is sufficiently large that its range is microscopic, then, on solar-system scales, the scalar field is suppressed, and the theory is essentially equivalent to general relativity. For a detailed review of scalar-tensor theories see [42].

### C. $f(R)$ theories

These are theories whose action has the form

$$I = \frac{c^3}{16\pi G} \int f(R)(-g)^{1/2} d^4x + I_{\text{m}}(\psi_{\text{m}}, g_{\mu\nu}), \quad (11)$$

where  $f$  is a function chosen so that at cosmological scales, the universe will experience accelerated expansion without resorting to either a cosmological constant or dark energy. However, it turns out that such theories are equivalent to scalar-tensor theories: replace  $f(R)$  by  $f(\chi) - f_{,\chi}(\chi)(R - \chi)$ , where  $\chi$  is a dynamical field. Varying the action with respect to  $\chi$  yields  $f_{,\chi\chi}(R - \chi) = 0$ , which implies that  $\chi = R$  as long as  $f_{,\chi\chi} \neq 0$ . Then defining a scalar field  $\phi \equiv f_{,\chi}(\chi)$  one puts the action into the form of a scalar-tensor theory given by Eq. (7), with  $\omega(\phi) = 0$  and  $\phi^2 V = \phi\chi(\phi) - f(\chi(\phi))$ . As we will see, this value of  $\omega$  would ordinarily strongly violate solar-system experiments, but it turns out that in many models, the potential  $V(\phi)$  has the effect of giving the scalar field a large effective mass in the presence of matter (the so-called “chameleon mechanism”), so that the scalar field is suppressed at distances that extend outside bodies like the Sun and Earth. In this way, with only modest fine tuning,  $f(R)$  theories can claim to obey standard tests, while providing interesting, non general-relativistic behavior on cosmic scales. For detailed reviews of this class of theories, see [43, 44].

### D. Vector-tensor theories

These theories contain the metric  $\mathbf{g}$  and a dynamical, typically timelike, four-vector field  $u^\mu$ . In some models, the four-vector is unconstrained, while in others, called Einstein-Æther theories it is constrained to be timelike with unit norm. The most general action for such theories that is quadratic in derivatives of the vector is given by

$$I = \frac{c^3}{16\pi G} \int \left[ (1 + \omega u_\mu u^\mu) R - K_{\alpha\beta}^{\mu\nu} \nabla_\mu u^\alpha \nabla_\nu u^\beta + \lambda(u_\mu u^\mu + 1) \right] \times (-g)^{1/2} d^4x + I_{\text{m}}(\psi_{\text{m}}, g_{\mu\nu}), \quad (12)$$

where

$$K_{\alpha\beta}^{\mu\nu} = c_1 g^{\mu\nu} g_{\alpha\beta} + c_2 \delta_\alpha^\mu \delta_\beta^\nu + c_3 \delta_\beta^\mu \delta_\alpha^\nu - c_4 u^\mu u^\nu g_{\alpha\beta}. \quad (13)$$

The coefficients  $c_i$  are arbitrary. In the unconstrained theories,  $\lambda \equiv 0$  and  $\omega$  is arbitrary. In the constrained theories,  $\lambda$  is a Lagrange multiplier, and by virtue of the constraint  $u_\mu u^\mu = -1$ , the factor  $\omega u_\mu u^\mu$  in front of the Ricci scalar can be absorbed into a rescaling of  $G$ ; equivalently, in the constrained theories, we can set  $\omega = 0$ . Note that the possible term  $u^\mu u^\nu R_{\mu\nu}$  can be shown under integration by parts to be equivalent to a linear combination of the terms involving  $c_2$  and  $c_3$ .

Unconstrained theories were studied during the 1970s as “straw-man” alternatives to general relativity. In addition to having up to four arbitrary parameters, they also left the magnitude of the vector field arbitrary, since it satisfies a linear homogenous vacuum field equation of the form  $\mathcal{L}u^\mu = 0$  ( $c_4 = 0$  in all such cases studied). Indeed, this latter fact was one of most serious defects of these theories.

#### General vector-tensor theory; $\omega, \tau, \epsilon, \eta$ (TEGP 5.4)

The gravitational Lagrangian for this class of theories had the form  $R + \omega u_\mu u^\mu R + \eta u^\mu u^\nu R_{\mu\nu} - \epsilon F_{\mu\nu} F^{\mu\nu} + \tau \nabla_\mu u_\nu \nabla^\mu u^\nu$ , where  $F_{\mu\nu} = \nabla_\mu u_\nu - \nabla_\nu u_\mu$ , corresponding to the values  $c_1 = 2\epsilon - \tau$ ,  $c_2 = -\eta$ ,  $c_1 + c_2 + c_3 = -\tau$ ,  $c_4 = 0$  and  $\lambda = 0$ . In these theories  $\gamma, \beta, \alpha_1$ , and  $\alpha_2$  are complicated functions of the parameters and of  $u^2 = -u^\mu u_\mu$ , while the rest vanish.

#### Will–Nordtvedt theory [37]

This is the special case  $c_1 = -1$ ,  $c_2 = c_3 = c_4 = \lambda = 0$ . In this theory, the PPN parameters are given by  $\gamma = \beta = 1$ ,  $\alpha_2 = u^2/(1 + u^2/2)$ , and zero for the rest.

#### Hellings–Nordtvedt theory; $\omega$ [45]

This is the special case  $c_1 = 2$ ,  $c_2 = 2\omega$ ,  $c_1 + c_2 + c_3 = 0 = c_4$ ,  $\lambda = 0$ . Here  $\gamma, \beta, \alpha_1$  and  $\alpha_2$  are complicated functions of the parameters and of  $u^2$ , while the rest vanish.

#### Einstein–Æther theories; $c_1, c_2, c_3, c_4$ [46–50]

These theories were motivated in part by a desire to explore possibilities for violations of Lorentz invariance in gravity, in parallel with similar studies in matter interactions, such as the SME. Here  $\gamma = \beta = 1$ ,  $\alpha_1$  and  $\alpha_2$  are complicated functions of the  $c_k$  parameters, and the rest vanish. By requiring that gravitational wave modes have real (as opposed to imaginary) frequencies, one can impose the bounds  $c_1/(c_1 + c_4) \geq 0$  and  $(c_1 + c_2 + c_3)/(c_1 + c_4) \geq 0$ . Considerations of positivity of energy impose the constraints  $c_1 > 0$ ,  $c_1 + c_4 > 0$  and  $c_1 + c_2 + c_3 > 0$ .

#### Khronometric theory; $\alpha_K, \beta_K, \lambda_K$ [51–54]

This is the low-energy limit of “Hořava gravity”, a proposal for a gravity theory that is power-counting renormalizable. The vector field is required to be hypersurface orthogonal, so that higher spatial derivative terms could be introduced to effectuate renormalizability. A “healthy” version of the theory can be shown to correspond to the values  $c_1 = -\epsilon$ ,  $c_2 = \lambda_K$ ,  $c_3 = \beta_K + \epsilon$  and  $c_4 = \alpha_K + \epsilon$ , where the limit  $\epsilon \rightarrow \infty$  is to be taken.

### E. Tensor-vector-scalar (TeVēS) theories

This class of theories was invented to provide a fully relativistic theory of gravity that could mimic the phenomenological behavior of so-called Modified Newtonian Dynamics (MOND), whereby in a weak-field regime, Newton’s laws hold, namely  $a = Gm/r^2$  where  $m$  is the mass of a central object, as long as  $a$  is small compared to some fundamental scale  $a_0$ , but in a regime where  $a > a_0$ , the equations of motion would take the form  $a^2/a_0 = Gm/r^2$ . With such a behavior, the rotational velocity of a particle far from a central mass would have the form  $v \sim \sqrt{ar} \sim (Gma_0)^{1/4}$ , thus reproducing the flat rotation curves observed for spiral galaxies, without invoking a distribution of dark matter.

Devising such a theory turned out to be no simple matter, and the final result, TeVeS was rather complicated [55]. Furthermore, it was shown to have unexpected singular behavior that was most simply cured by incorporating features of the Einstein–Æther theory [56]. The extended theory is based on an “Einstein” metric  $\tilde{g}_{\mu\nu}$ , related to the physical metric  $g_{\mu\nu}$  by

$$g_{\mu\nu} \equiv e^{-2\phi} \tilde{g}_{\mu\nu} - 2u_\mu u_\nu \sinh(2\phi), \quad (14)$$

where  $u^\mu$  is a vector field, and  $\phi$  is a scalar field. The action for gravity is the standard general relativity action of Eq. (3), but defined using the Einstein metric  $\tilde{g}_{\mu\nu}$ , while the matter action is that of a standard metric theory, using  $g_{\mu\nu}$ .

These are supplemented by the vector action, given by that of Einstein-Æther theory, Eq. (12), and a scalar action, given by

$$I_S = -\frac{c^3}{2k^2\ell^2G} \int \mathcal{F}(k\ell^2 h^{\mu\nu} \phi_{,\mu} \phi_{,\nu}) (-g)^{1/2} d^4x, \quad (15)$$

where  $k$  is a constant,  $\ell$  is a distance, and  $h^{\mu\nu} \equiv \tilde{g}^{\mu\nu} - u^\mu u^\nu$ , indices being raised and lowered using the Einstein metric. The function  $\mathcal{F}(y)$  is chosen so that  $\mu(y) \equiv d\mathcal{F}/dy$  is unity in the high-acceleration, or normal Newtonian regime, and nearly zero in the MOND regime.

The PPN parameters of the theory [57] have the values  $\gamma = \beta = 1$  and  $\xi = \alpha_3 = \zeta_i = 0$ , while the parameters  $\alpha_1$  and  $\alpha_2$  are complicated functions of  $k$ ,  $c_k$  and the asymptotic value  $\phi_0$  of the scalar field.

For reviews of TeVeS, MOND and their confrontation with the dark-matter paradigm, see [58, 59].

## F. Other theories

Numerous alternative theories of gravity have been developed and studied extensively in recent years, most motivated from the direction of particle physics, quantum gravity or unification.

Massive gravity theories attempt to give the putative “graviton” a mass. The simplest attempts fall afoul of the so-called van Dam-Veltman-Zakharov discontinuity, which leads to a violation of experiment. Attempts to avoid this problem involve treating non-linear aspects of the theory at the fundamental level; many models incorporate a second tensor field in addition to the metric. For a recent review, see [60]. Quadratic gravity is a recent incarnation of an old idea of adding to the action of general relativity terms quadratic in the Riemann and Ricci tensors or the Ricci scalar, as an effective model for quantum gravity corrections. Chern-Simons gravity adds a parity-violating term proportional to  $*R^{\alpha\beta\gamma\delta} R_{\alpha\beta\gamma\delta}$  to the action of general relativity, where  $*R^{\alpha\beta\gamma\delta}$  is the dual Riemann tensor.

## V. TESTS OF POST-NEWTONIAN GRAVITY

### A. Tests of the parameter $\gamma$

With the PPN formalism in hand, we are now ready to confront gravitation theories described in Sec. IV with the results of solar-system experiments. In this section we focus on tests of the parameter  $\gamma$ , consisting of the deflection of light and the time delay of light.

#### 1. The deflection of light

A light ray (or photon) which passes the Sun at a distance  $d$  is deflected by an angle

$$\delta\theta = \frac{1}{2}(1 + \gamma) \frac{4GM_\odot}{dc^2} \frac{1 + \cos\Phi}{2} \quad (16)$$

(TEGP 7.1), where  $M_\odot$  is the mass of the Sun and  $\Phi$  is the angle between the Earth-Sun line and the incoming direction of the photon. For a grazing ray,  $d \approx d_\odot$ ,  $\Phi \approx 0$ , and

$$\delta\theta \approx \frac{1}{2}(1 + \gamma) 1.''7505, \quad (17)$$

independent of the frequency of light. In practice, one measures how the relative angular separation between an observed source of light and a nearby reference source evolves as the Sun moves across the sky, as seen from Earth.

It is interesting to note that the classic derivations of the deflection that use only the corpuscular theory of light, by Cavendish in 1784 and von Soldner in 1803 [61], or that use only the principle of equivalence, by Einstein in 1911, yield only the “1/2” part of the coefficient in front of the expression in Eq. (16). But the result of these calculations is the deflection of light relative to local straight lines, as established for example by rigid rods; however, because of space curvature around the Sun, determined by the PPN parameter  $\gamma$ , local straight lines are bent relative to asymptotic straight lines far from the Sun by just enough to yield the remaining factor “ $\gamma/2$ ”. The first factor “1/2” holds in any metric theory, the second “ $\gamma/2$ ” varies from theory to theory. Thus, calculations that purport to derive the full deflection using the equivalence principle alone are incorrect.

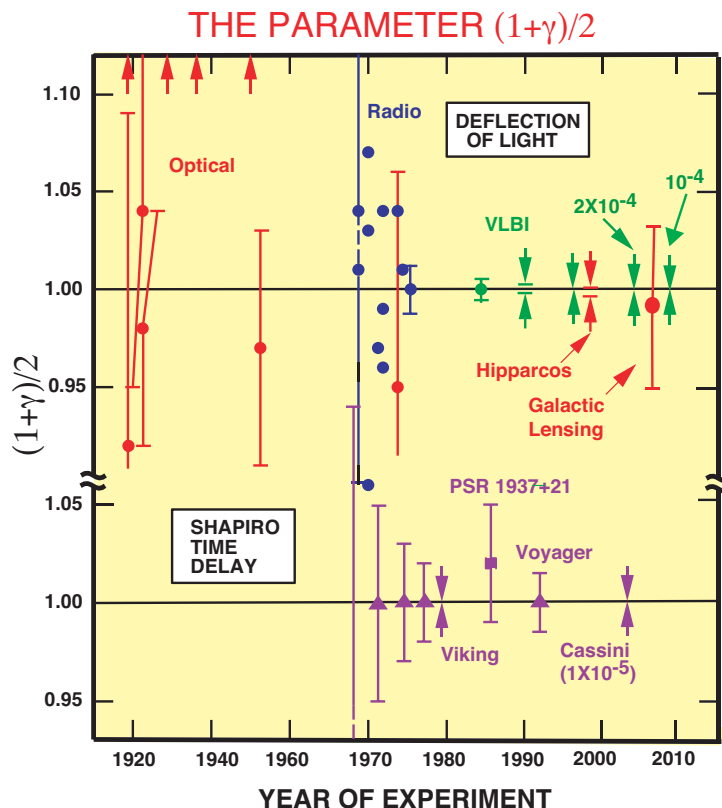


FIG. 4: Measurements of the coefficient  $(1 + \gamma)/2$  from light deflection and time delay measurements. Its general relativity value is unity. The arrows at the top denote anomalously large values from early eclipse expeditions. The Shapiro time-delay measurements using the Cassini spacecraft yielded an agreement with general relativity to  $10^{-3}$  percent, and VLBI light deflection measurements have reached 0.02 percent. Hipparcos denotes the optical astrometry satellite, which reached 0.1 percent.

The prediction of the full bending of light by the Sun was one of the great successes of Einstein’s general relativity. Eddington’s confirmation of the bending of optical starlight observed during a solar eclipse in the first days following World War I helped make Einstein famous. However, the experiments of Eddington and his co-workers had only 30 percent accuracy, and succeeding experiments were not much better: The results were scattered between one half and twice the Einstein value (see Figure 4), and the accuracies were low.

However, the development of radio interferometry, and later of very-long-baseline radio interferometry (VLBI), produced greatly improved determinations of the deflection of light. These techniques now have the capability of measuring angular separations and changes in angles to accuracies better than 100 microarcseconds. Early measurements took advantage of the fact that certain groups of strong quasistellar radio sources annually pass very close to the Sun (as seen from the Earth), and by 1975 were reaching accuracies at the level of a percent.

In recent years, transcontinental and intercontinental VLBI observations of quasars and radio galaxies have been made primarily to monitor the Earth’s rotation (“VLBI” in Figure 4). These measurements are sensitive to the deflection of light over almost the entire celestial sphere (at  $90^\circ$  from the Sun, the deflection is still 4 milliarcseconds). A 2004 analysis of almost 2 million VLBI observations of 541 radio sources, made by 87 VLBI sites between 1979 and 1999 yielded  $(1 + \gamma)/2 = 0.99992 \pm 0.00023$ , or equivalently,  $\gamma - 1 = (-1.7 \pm 4.5) \times 10^{-4}$  [62]. Analyses that incorporated data through 2010 yielded  $\gamma - 1 = (-0.8 \pm 1.2) \times 10^{-4}$  [63].

Analysis of observations made by the Hipparcos optical astrometry satellite yielded a test at the level of 0.3 percent, while the GAIA mission, launched in 2013, is expected to reach the parts per million level.

Finally, a remarkable measurement of  $\gamma$  on galactic scales was reported in 2006 [64]. It used data on gravitational lensing by 15 elliptical galaxies, collected by the Sloan Digital Sky Survey. The Newtonian potential  $U$  of each lensing galaxy (including the contribution from dark matter) was derived from the observed velocity dispersion of stars in the galaxy. Comparing the observed lensing with the lensing predicted by the models provided a 10 percent bound on  $\gamma$ , in agreement with general relativity. Unlike the much tighter bounds described previously, which were obtained



on the scale of the solar system, this bound was obtained on a galactic scale.

The results of light-deflection measurements are summarized in Figure 4.

## 2. The time delay of light

A radar signal sent across the solar system past the Sun to a planet or satellite and returned to the Earth suffers an additional non-Newtonian delay in its round-trip travel time, given by

$$\delta t = 2(1 + \gamma) \frac{GM_{\odot}}{c^3} \ln \left( \frac{(r_{\oplus} + \mathbf{x}_{\oplus} \cdot \mathbf{n})(r_e - \mathbf{x}_e \cdot \mathbf{n})}{d^2} \right), \quad (18)$$

where  $\mathbf{x}_e$  ( $\mathbf{x}_{\oplus}$ ) are the vectors, and  $r_e$  ( $r_{\oplus}$ ) are the distances from the Sun to the source (Earth), respectively (TEGP 7.2). For a ray which passes close to the Sun,

$$\delta t \approx \frac{1}{2}(1 + \gamma) \left( 240 - 20 \ln \frac{d^2}{r} \right) \mu\text{s}, \quad (19)$$

where  $d$  is the distance of closest approach of the ray in solar radii, and  $r$  is the distance of the planet or satellite from the Sun, in astronomical units.

In the two decades following Irwin Shapiro's 1964 discovery of this effect as a theoretical consequence of general relativity, several high-precision measurements were made using radar ranging to targets passing through superior conjunction. Since one does not have access to a "Newtonian" signal against which to compare the round-trip travel time of the observed signal, it is necessary to do a differential measurement of the variations in round-trip travel times as the target passes through superior conjunction, and to look for the logarithmic behavior of Equation (19). In order to do this accurately however, one must take into account the variations in round-trip travel time due to the orbital motion of the target relative to the Earth. This is done by using radar-ranging (and possibly other) data on the target taken when it is far from superior conjunction (i.e. when the time-delay term is negligible) to determine an accurate ephemeris for the target, using the ephemeris to predict the PPN coordinate trajectory  $\mathbf{x}_e(t)$  near superior conjunction, then combining that trajectory with the trajectory of the Earth  $\mathbf{x}_{\oplus}(t)$  to determine the Newtonian round-trip time and the logarithmic term in Equation (19). The resulting predicted round-trip travel times in terms of the unknown coefficient  $\frac{1}{2}(1 + \gamma)$  are then fit to the measured travel times using the method of least-squares, and an estimate obtained for  $\frac{1}{2}(1 + \gamma)$ .

The targets employed included planets, such as Mercury or Venus, used as passive reflectors of the radar signals, and artificial satellites, such as Mariners 6 and 7, Voyager 2, the Viking Mars landers and orbiters, and the Cassini spacecraft to Saturn, used as active retransmitters of the radar signals.

The results for the coefficient  $\frac{1}{2}(1 + \gamma)$  of all radar time-delay measurements performed to date (including a measurement of the one-way time delay induced by the Sun on signals from the millisecond pulsar PSR 1937+21) are shown in Figure 4.

The best bound comes from Doppler tracking of the Cassini spacecraft while it was on its way to Saturn [65], with a result  $\gamma - 1 = (2.1 \pm 2.3) \times 10^{-5}$ . This was made possible by the ability to do Doppler measurements using both X-band (7175 MHz) and Ka-band (34316 MHz) radar, thereby significantly reducing the dispersive effects of the solar corona. In addition, the 2002 superior conjunction of Cassini was particularly favorable: with the spacecraft at 8.43 astronomical units from the Sun, the distance of closest approach of the radar signals to the Sun was only  $1.6 R_{\odot}$ .

The Shapiro time delay plays a key role in determining the parameters of binary pulsar orbits, notably in the "double pulsar" system (see Sec. VIB).

## B. The perihelion shift of Mercury

The explanation of the anomalous perihelion shift of Mercury's orbit was another of the triumphs of general relativity. This had been an unsolved problem in celestial mechanics for over half a century, since the announcement by Le Verrier in 1859 that, after the perturbing effects of the planets on Mercury's orbit had been accounted for, there remained an unexplained advance in the perihelion of Mercury. The modern value for this discrepancy is 42.98 arcseconds per century. A number of *ad hoc* proposals were made in an attempt to account for this excess, including, the existence of a new planet Vulcan near the Sun, a ring of planetoids, a solar quadrupole moment and a deviation from the inverse-square law of gravitation, but none was successful. General relativity accounted for the anomalous shift in a natural way without disturbing the agreement with other planetary observations.

TABLE IV: Current limits on the PPN parameters.

Parameter	Effect	Limit	Remarks
$\gamma - 1$	time delay	$2.3 \times 10^{-5}$	Cassini tracking
	light deflection	$2 \times 10^{-4}$	VLBI
$\beta - 1$	perihelion shift	$8 \times 10^{-5}$	$J_{2\odot} = (2.2 \pm 0.1) \times 10^{-7}$
	Nordtvedt effect	$2.3 \times 10^{-4}$	$\eta_N = 4\beta - \gamma - 3$ assumed
$\xi$	spin precession	$4 \times 10^{-9}$	millisecond pulsars
$\alpha_1$	orbital polarization	$10^{-4}$	Lunar laser ranging
		$4 \times 10^{-5}$	PSR J1738+0333
$\alpha_2$	spin precession	$2 \times 10^{-9}$	millisecond pulsars
$\alpha_3$	pulsar acceleration	$4 \times 10^{-20}$	pulsar $\dot{P}$ statistics
$\zeta_1$	—	$2 \times 10^{-2}$	combined PPN bounds
$\zeta_2$	binary acceleration	$4 \times 10^{-5}$	$\ddot{P}_p$ for PSR 1913+16
$\zeta_3$	Newton's 3rd law	$10^{-8}$	lunar acceleration
$\zeta_4$	—	—	not independent

The predicted advance per orbit  $\Delta\tilde{\omega}$ , including both relativistic PPN contributions and the Newtonian contribution resulting from a possible solar quadrupole moment, is given by

$$\Delta\tilde{\omega} = 6\pi \frac{Gm}{pc^2} \left( \frac{2 + 2\gamma - \beta}{3} \right) + 3\pi J_2 \left( \frac{R}{p} \right)^2, \quad (20)$$

where  $m$  is the total mass of the Sun-Mercury system;  $p \equiv a(1 - e^2)$  is the semi-latus rectum of the orbit, with the semi-major axis  $a$  and the eccentricity  $e$ ;  $R$  is the mean radius of the Sun; and  $J_2$  is a dimensionless measure of its quadrupole moment (for details of the derivation see TEGP 7.3). We have here restricted attention to fully-conservative theories of gravity.

Through observations of the normal modes of solar oscillations (helioseismology) it is now known that  $J_2 = (2.2 \pm 0.1) \times 10^{-7}$ , comparable to what would be estimated from a uniformly rotating solar model. Substituting standard orbital elements and physical constants for Mercury and the Sun we obtain the rate of perihelion shift  $\dot{\tilde{\omega}}$ , in seconds of arc per century,

$$\dot{\tilde{\omega}} = 42.''98 \left( \frac{2 + 2\gamma - \beta}{3} + 3 \times 10^{-4} \frac{J_2}{10^{-7}} \right). \quad (21)$$

The most recent fits to planetary data include data from the Messenger spacecraft that orbited Mercury, thereby significantly improving knowledge of its orbit. Adopting the Cassini bound on  $\gamma$  *a priori*, these analyses yield a bound on  $\beta$  given by  $|\beta - 1| = (-4.1 \pm 7.8) \times 10^{-5}$  [66, 67]. Further analysis could push this bound even lower, although knowledge of  $J_2$  would have to improve simultaneously.

Laser tracking of the Earth-orbiting satellite LAGEOS II led to a measurement of its relativistic perigee precession (3.4 arcseconds per year) in agreement with general relativity to two percent [68].

### C. Tests of the strong equivalence principle

The next class of solar-system experiments that test relativistic gravitational effects may be called tests of the strong equivalence principle (SEP). In Sec. IIB we pointed out that many metric theories of gravity (perhaps all except general relativity) can be expected to violate one or more aspects of SEP. Among the testable violations of SEP are a violation of the weak equivalence principle for gravitating bodies that leads to perturbations in the Earth-Moon orbit, preferred-location and preferred-frame effects in orbital dynamics or in the structure of bodies such as the Earth, and possible variations in the gravitational constant over cosmological timescales.

### 1. The Nordtvedt effect

In a pioneering calculation using his early form of the PPN formalism, Kenneth Nordtvedt [69] showed that many metric theories of gravity predict that massive bodies violate the weak equivalence principle – that is, fall with different accelerations depending on their gravitational self-energy. Dicke [70] argued that such an effect would occur in theories with a spatially varying gravitational constant, such as scalar-tensor gravity. In the PPN framework, the acceleration of a massive body in an external gravitational potential  $U$  has the form

$$\begin{aligned} \mathbf{a} &= \left(1 - \eta_N \frac{E_g}{mc^2}\right) \nabla U, \\ \eta_N &= 4\beta - \gamma - 3 - \frac{10}{3}\xi - \alpha_1 + \frac{2}{3}\alpha_2 - \frac{2}{3}\zeta_1 - \frac{1}{3}\zeta_2, \end{aligned} \tag{22}$$

where  $E_g$  is the negative of the gravitational self-energy of the body ( $E_g > 0$ ). This violation of the massive-body equivalence principle is known as the “Nordtvedt effect”. The effect is absent in general relativity ( $\eta_N = 0$ ) but present in scalar-tensor theory ( $\eta_N = (1 + 2\lambda)/(2 + \omega)$ ). The existence of the Nordtvedt effect does not violate the results of laboratory Eötvös experiments, since for laboratory-sized objects  $E_g/mc^2 \leq 10^{-27}$ , far below the sensitivity of current or future experiments. However, for astronomical bodies,  $E_g/mc^2$  may be significant ( $3.6 \times 10^{-6}$  for the Sun,  $4.6 \times 10^{-10}$  for the Earth,  $0.2 \times 10^{-10}$  for the Moon,  $\sim 0.2$  for neutron stars). If the Nordtvedt effect is present ( $\eta_N \neq 0$ ) then the Earth should fall toward the Sun with a slightly different acceleration than the Moon. This perturbation in the Earth-Moon orbit leads to a polarization of the orbit that is directed toward the Sun as it moves around the Earth-Moon system, as seen from Earth. This polarization represents a perturbation in the Earth-Moon distance of the form  $\delta r = 13.1 \eta_N \cos[(\omega_0 - \omega_s)t]$  meters, where  $\omega_0$  and  $\omega_s$  are the angular frequencies of the orbits of the Moon and Sun around the Earth (see TEGP 8.1 for detailed derivations).

Since August 1969, when the first successful acquisition was made of a laser signal reflected from the Apollo 11 retroreflector on the Moon, the LLR experiment has made regular measurements of the round-trip travel times of laser pulses between a network of observatories and the lunar retroreflectors, with accuracies that are approaching the 5 ps (1 mm) level. These measurements are fit using the method of least-squares to a theoretical model for the lunar motion that takes into account perturbations due to the Sun and the other planets, tidal interactions, and post-Newtonian gravitational effects. The predicted round-trip travel times between retroreflector and telescope also take into account the librations of the Moon, the orientation of the Earth, the location of the observatories, and atmospheric effects on the signal propagation. The “Nordtvedt” parameter  $\eta_N$  along with several other important parameters of the model are then estimated in the least-squares method. For a review of lunar laser ranging, see [71].

Numerous ongoing analyses of the data find no evidence, within experimental uncertainty, for the Nordtvedt effect [72]. These results represent a limit on a possible violation of WEP for massive bodies of about 1.4 parts in  $10^{13}$  (compare Figure 1).

However, at this level of precision, one cannot regard the results of LLR as a “clean” test of SEP until one eliminates the possibility of a compensating violation of WEP for the two bodies, because the chemical compositions of the Earth and Moon differ in the relative fractions of iron and silicates. To this end, the Eöt-Wash group carried out an improved test of WEP for laboratory bodies whose chemical compositions mimic that of the Earth and Moon. The resulting bound of 1.4 parts in  $10^{13}$  [73] from composition effects reduces the ambiguity in the LLR bound, and establishes the firm SEP test at the level of about 2 parts in  $10^{13}$ . These results can be summarized by the Nordtvedt parameter bound  $|\eta_N| = (4.4 \pm 4.5) \times 10^{-4}$ .

APOLLO, the Apache Point Observatory for Lunar Laser ranging Operation, a joint effort by researchers from the Universities of Washington, Seattle, and California, San Diego, has achieved mm ranging precision using enhanced laser and telescope technology, together with a good, high-altitude site in New Mexico. However models of the lunar orbit must be improved in parallel in order to achieve an order-of-magnitude improvement in the test of the Nordtvedt effect [74]. This effort will be aided by the fortuitous 2010 discovery by the Lunar Reconnaissance Orbiter of the precise landing site of the Soviet Lunokhod I rover, which deployed a retroreflector in 1970. Its uncertain location made it effectively “lost” to lunar laser ranging for almost 40 years. Its location on the lunar surface will make it useful in improving models of the lunar libration.

Tests of the Nordtvedt effect for neutron stars have also been carried out using a class of systems known as wide-orbit binary millisecond pulsars (WBMSPs), which are pulsar–white-dwarf binary systems with very small orbital eccentricities. In the gravitational field of the galaxy, a non-zero Nordtvedt effect can induce an apparent anomalous eccentricity pointed toward the galactic center, which can be bounded using statistical methods, given enough WBMSPs. Using data from 21 WBMSPs, including recently discovered highly circular systems, Stairs et al. [75] obtained the bound  $\Delta < 5.6 \times 10^{-3}$ , where  $\Delta = \eta_N (E_g/M)_{\text{NS}}$ . Because  $(E_g/M)_{\text{NS}} \sim 0.1$  for typical neutron stars, this bound does not compete with the bound on  $\eta_N$  from LLR; on the other hand, it does test SEP in the strong-field regime

TABLE V: Constancy of the gravitational constant.

Method	$\dot{G}/G$ ( $10^{-13} \text{ yr}^{-1}$ )	Reference
Mars ephemeris	$0.1 \pm 1.6$	[80]
Lunar laser ranging	$4 \pm 9$	[81]
Binary pulsars	$-7 \pm 33$	[82, 83]
Helioseismology	$0 \pm 16$	[84]
Big Bang nucleosynthesis	$0 \pm 4$	[85, 86]

because of the presence of the neutron star in each system. The 2013 discovery of a millisecond pulsar in orbit with *two* white dwarfs in very circular, coplanar orbits [76] may lead to a test of the Nordtvedt effect in the strong-field regime that surpasses the precision of lunar laser ranging by a substantial factor.

### 2. Preferred-frame and preferred-location effects

Some theories of gravity violate SEP by predicting that the outcomes of local gravitational experiments may depend on the velocity of the laboratory relative to the mean rest frame of the universe (preferred-frame effects) or on the location of the laboratory relative to a nearby gravitating body (preferred-location effects). In the post-Newtonian limit, preferred-frame effects are governed by the values of the PPN parameters  $\alpha_1$ ,  $\alpha_2$ , and  $\alpha_3$ , and some preferred-location effects are governed by  $\xi$  (see Table II).

The most important such effects are variations and anisotropies in the locally-measured value of the gravitational constant which lead to anomalous Earth tides and variations in the Earth’s rotation rate, anomalous contributions to the orbital dynamics of planets, the Moon and binary pulsars; self-accelerations of isolated pulsars; and anomalous torques on spinning bodies such as the Sun or pulsars (see TEGP 8.2, 8.3, 9.3, and 14.3 (c)). A tight bound on  $\alpha_3$  was obtained from the period derivatives of 21 millisecond pulsars [75]. The best bound on  $\alpha_1$ , comes from the orbit of the pulsar–white-dwarf system J1738+0333; while the best bounds on  $\alpha_2$  and  $\xi$  come from bounding torques on the solitary millisecond pulsars B1937+21 and J1744–1134 [77–79]. Because these bounds involved systems with strong internal gravity of the neutron stars, they should strictly speaking be regarded as bounds on “strong field” analogues of the PPN parameters. Here we will treat them as bounds on the standard PPN parameters, as shown in Table IV.

### 3. Constancy of the Newtonian gravitational constant

Most theories of gravity that violate SEP predict that the locally measured Newtonian gravitational constant may vary with time as the universe evolves. For the scalar-tensor theories listed in Table III, for example, the predictions for  $\dot{G}/G$  can be written in terms of time derivatives of the asymptotic scalar field. Where  $G$  does change with cosmic evolution, its rate of variation should be related to the expansion rate of the universe, i.e.  $\dot{G}/G \sim H_0$ , where  $H_0$  is the Hubble expansion parameter and is given by  $H_0 = 73 \pm 3 \text{ km s}^{-1} \text{ Mpc}^{-1} \approx 0.75 \times 10^{-10} \text{ yr}^{-1}$ .

Several observational constraints can be placed on  $\dot{G}/G$ , one kind coming from bounding the present rate of variation, another from bounding a difference between the present value and a past value. The first type of bound typically comes from LLR measurements, planetary radar-ranging measurements, and pulsar timing data. The best limits come from improvements in the ephemeris of Mars using range and Doppler data from the Mars Global Surveyor (1998–2006), Mars Odyssey (2002–2008), and Mars Reconnaissance Orbiter (2006–2008), together with improved data and modeling of the effects of the asteroid belt [80]. Since the bound is actually on variations of  $GM_\odot$ , any future improvements in  $\dot{G}/G$  beyond a part in  $10^{13}$  will have to take into account models of the actual mass loss from the Sun, due to radiation of light and neutrinos ( $\sim 0.7 \times 10^{-13} \text{ yr}^{-1}$ ) and due to the solar wind ( $\sim 0.2 \times 10^{-13} \text{ yr}^{-1}$ ). The second type of bound comes from studies of the evolution of the Sun, stars and the Earth, big-bang nucleosynthesis, and analyses of ancient eclipse data. Selected results are shown in Table V; a thorough review is given in [27].

#### D. The search for gravitomagnetism

According to general relativity, moving or rotating matter should produce a contribution to the gravitational field that is the analogue of the magnetic field of a moving charge or a magnetic dipole. From the geometrical point of view, rotating matter produces a “dragging of inertial frames” around the body, also called the Lense–Thirring effect. One consequence of this phenomenon is a precession of a gyroscope’s spin  $\mathbf{S}$  according to

$$\frac{d\mathbf{S}}{dt} = \boldsymbol{\Omega}_{\text{LT}} \times \mathbf{S}, \quad \boldsymbol{\Omega}_{\text{LT}} = -\frac{1}{2} \left( 1 + \gamma + \frac{1}{4}\alpha_1 \right) \frac{G(\mathbf{J} - 3\mathbf{n}(\mathbf{n} \cdot \mathbf{J}))}{c^2 r^3}, \quad (23)$$

where  $\mathbf{n}$  is a unit radial vector, and  $r$  is the distance from the center of the body with angular momentum  $\mathbf{J}$  (TEGP 9.1).

Another effect on the spin of a gyroscope arises from curved spacetime around the central body, called the “geodetic precession”, given by

$$\frac{d\mathbf{S}}{d\tau} = \boldsymbol{\Omega}_{\text{G}} \times \mathbf{S}, \quad \boldsymbol{\Omega}_{\text{G}} = \left( \gamma + \frac{1}{2} \right) \frac{\mathbf{v} \times \nabla U}{c^2}, \quad (24)$$

where  $\mathbf{v}$  is the velocity of the gyroscope, and  $U$  is the Newtonian gravitational potential of the source (TEGP 9.1).

The Relativity Gyroscope Experiment (Gravity Probe B or GPB) carried out by Stanford University, NASA and Lockheed–Martin Corporation, was a space mission designed to detect both precessional effects. Gravity Probe B will very likely go down in the history of science as one of the most ambitious, difficult, expensive, and controversial relativity experiments ever performed.<sup>2</sup> It was almost 50 years from inception to completion, although only about half of that time was spent as a full-fledged, approved space program.

The GPB spacecraft was launched on April 20, 2004 into an almost perfectly circular polar orbit at an altitude of 642 km, with the orbital plane parallel to the direction of a guide star known as *IM Pegasi* (HR 8703). The spacecraft contained four spheres made of fused quartz, all spinning about the same axis (two were spun in the opposite direction), which was oriented to be in the orbital plane, pointing toward the guide star. An onboard telescope pointed continuously at the guide star, and the direction of each spin was compared with the direction to the star, which was at a declination of 16° relative to the Earth’s equatorial plane. With these conditions, the predicted precessions were 6630 milliarcsecond per year for the geodetic effect, and 38 milliarcsecond per year for frame dragging, the former in the orbital plane (in the north-south direction) and the latter perpendicular to it (in the east-west direction).

In order to reduce the non-relativistic torques on the rotors to an acceptable level, the rotors were fabricated to be both spherical and homogenous to better than a few parts in 10 million. Each rotor was coated with a thin film of niobium, and the experiment was conducted at cryogenic temperatures inside a dewar containing 2200 litres of superfluid liquid helium. As the niobium film becomes a superconductor, each rotor develops a magnetic moment parallel to its spin axis. Variations in the direction of the magnetic moment relative to the spacecraft were then measured using superconducting current loops surrounding each rotor. As the spacecraft orbits the Earth, the aberration of light from the guide star causes an artificial but predictable change in direction between the rotors and the on-board telescope; this was an essential tool for calibrating the conversion between the voltages read by the current loops and the actual angle between the rotors and the guide star.

The mission ended in September 2005, as scheduled, when the last of the liquid helium boiled off. Although all subsystems of the spacecraft and the apparatus performed extremely well, they were not perfect. Calibration measurements carried out during the mission, both before and after the science phase, revealed unexpectedly large torques on the rotors. Numerous diagnostic tests worthy of a detective novel showed that these were caused by electrostatic interactions between surface imperfections (“patch effect”) on the niobium films and the spherical housings surrounding each rotor. These effects and other anomalies greatly contaminated the data and complicated its analysis, but finally, in October 2010, the Gravity Probe B team announced that the experiment had successfully measured both the geodetic and frame-dragging precessions. The outcome was in agreement with general relativity, with a precision of 0.3 percent for the geodetic precession, and 20 percent for the frame-dragging effect [87].

Another way to look for frame-dragging is to measure the precession of orbital planes of bodies circling a rotating body. One implementation of this idea is to measure the relative precession, at about 31 milliarcseconds per year, of the line of nodes of a pair of laser-ranged geodynamics satellites (LAGEOS), ideally with supplementary inclination angles; the inclinations must be supplementary in order to cancel the huge (126 degrees per year) nodal precession caused by the Earth’s Newtonian gravitational multipole moments. Unfortunately, the two existing LAGEOS satellites

---

<sup>2</sup> Full disclosure: The author served as Chair of an external NASA Science Advisory Committee for Gravity Probe B from 1998 to 2010.

are not in appropriately inclined orbits. Nevertheless, Ciufolini et al. [88, 89] combined nodal precession data from LAGEOS I and II with improved models for the Earth’s multipole moments provided by two recent orbiting geodesy satellites, Europe’s CHAMP (Challenging Minisatellite Payload) and NASA’s GRACE (Gravity Recovery and Climate Experiment), and reported a 5–10 percent confirmation of general relativity.

On February 13, 2012, a third laser-ranged satellite, known as LARES (Laser Relativity Satellite) was launched by the Italian Space Agency. Its inclination was very close to the required supplementary angle relative to LAGEOS I, and its eccentricity was very nearly zero. However, because its semimajor axis is only 2/3 that of either LAGEOS I or II, and because the Newtonian precession rate is proportional to  $a^{-3/2}$ , LARES does not provide a cancellation of the Newtonian precession. Combining data from all three satellites with continually improving Earth data from GRACE, the LARES team hopes to achieve a test of frame-dragging at the one percent level.

## VI. BINARY-PULSAR TESTS OF GRAVITATIONAL THEORY

The 1974 discovery of the binary pulsar B1913+16 by Joseph Taylor and Russell Hulse during a routine search for new pulsars was a milestone in the history of general relativity. It led to the first confirmation of the existence of gravitational radiation and to a Nobel Prize for Taylor and Hulse, and it opened a new field for testing gravitational theories in the strong-field and gravitational-wave regimes.

Following that discovery, only two new binary pulsars were discovered with interesting relativistic properties during the next 15 years (out of a total of 14 systems), but thanks to improved radio-telescope sensitivity, better techniques for removing the effects of interstellar dispersion, better timing capabilities (exploiting GPS time transfer, for example) and improved detection algorithms, the pace of discovery of binary pulsars picked up steadily. Today, over 220 binary pulsars are known, with 23 discovered in 2012 alone. To be sure, the vast majority of these are of little relativistic interest, either because they are so widely separated that relativistic effects are negligible, because they involve significant mass-transfer from the companion (X-ray binary pulsars), or because the timing characteristics of the pulsar do not meet the stability demanded to measure relativistic effects.

Nevertheless, close to a dozen binary pulsars are relativistically interesting for one reason or another, and this zoo of systems contains some fascinating beasts, including the famous “double pulsar”, systems with white-dwarf companions, a system with the most massive neutron star known, and systems with extraordinarily circular orbits.

### A. The binary pulsar and general relativity

We will begin by reviewing the iconic Hulse-Taylor binary pulsar, by far the best studied of all the systems. Pulse arrival-time measurements have been made regularly (apart from a four-year break during upgrading of the Arecibo radio telescope) for over 30 years. Table VI lists the current values of the key orbital and relativistic parameters, from analysis of data through 2006 [90].

The observational parameters that are obtained from a least-squares solution of the arrival-time data fall into three groups:

1. non-orbital parameters, such as the pulsar period and its rate of change (defined at a given epoch), and the position of the pulsar on the sky;
2. five “Keplerian” parameters, most closely related to those appropriate for standard Newtonian binary systems, such as the eccentricity  $e$ , the orbital period  $P_b$ , and the semi-major axis of the pulsar projected along the line of sight,  $a_p \sin i$ ; and
3. five “post-Keplerian” parameters.

The five post-Keplerian parameters are:  $\langle \dot{\omega} \rangle$ , the average rate of periastron advance;  $\gamma'$ , the amplitude of delays in arrival of pulses caused by the varying effects of the gravitational redshift and time dilation as the pulsar moves in its elliptical orbit at varying distances from the companion and with varying speeds (not to be confused with the PPN parameter  $\gamma$ );  $\dot{P}_b$ , the rate of change of orbital period, caused predominantly by gravitational radiation damping; and  $r$  and  $s = \sin i$ , respectively the “range” and “shape” of the Shapiro time delay of the pulsar signal as it propagates through the curved spacetime region near the companion, where  $i$  is the angle of inclination of the orbit relative to the plane of the sky. An additional 14 relativistic parameters are measurable in principle [91].

TABLE VI: Parameters of the binary pulsar B1913+16. The numbers in parentheses denote errors in the last digit.

Parameter	Symbol (units)	Value
(i) Astrometric and spin parameters:		
Right Ascension	$\alpha$	$19^{\text{h}}15^{\text{m}}27.^{\text{s}}99928(9)$
Declination	$\delta$	$16^{\circ}06'27.''3871(13)$
Pulsar period	$P_{\text{p}}$ (ms)	$59.0299983444181(5)$
Derivative of period	$\dot{P}_{\text{p}}$	$8.62713(8) \times 10^{-18}$
(ii) “Keplerian” parameters:		
Projected semimajor axis	$a_{\text{p}} \sin i$ (s)	$2.341782(3)$
Eccentricity	$e$	$0.6171334(5)$
Orbital period	$P_{\text{b}}$ (day)	$0.322997448911(4)$
Longitude of periastron	$\omega_0$ ( $^{\circ}$ )	$292.54472(6)$
Julian date of periastron	$T_0$ (MJD)	$52144.90097841(4)$
(iii) “Post-Keplerian” parameters:		
Mean rate of periastron advance	$\langle \dot{\omega} \rangle$ ( $^{\circ} \text{ yr}^{-1}$ )	$4.226598(5)$
Redshift/time dilation	$\gamma'$ (ms)	$4.2992(8)$
Orbital period derivative	$\dot{P}_{\text{b}}$ ( $10^{-12}$ )	$-2.423(1)$

In general relativity, the five post-Keplerian parameters can be related to the masses of the two bodies and to measured Keplerian parameters by the equations (TEGP 12.1, 14.6 (a))

$$\langle \dot{\omega} \rangle = \frac{6\pi}{P_{\text{b}}} \left( \frac{2\pi G m \omega_{\text{b}}}{c^3} \right)^{2/3} \frac{1}{1 - e^2}, \quad (25)$$

$$\gamma' = e \frac{P_{\text{b}}}{2\pi} \left( \frac{2\pi G m \omega_{\text{b}}}{c^3} \right)^{2/3} \frac{m_2}{m} \left( 1 + \frac{m_2}{m} \right), \quad (26)$$

$$\dot{P}_{\text{b}} = -\frac{192\pi}{5} \left( \frac{2\pi G \mathcal{M} \omega_{\text{b}}}{c^3} \right)^{5/3} F(e), \quad (27)$$

$$s = \sin i, \quad (28)$$

$$r = m_2, \quad (29)$$

where  $\omega_{\text{b}} \equiv 2\pi/P_{\text{b}}$  is the orbital angular frequency;  $m_1$  and  $m_2$  are the pulsar and companion masses, respectively;  $m$  is the total mass;  $\mathcal{M}$  is the so-called “chirp” mass, given by  $\mathcal{M} \equiv (m_1 m_2 / m^2)^{3/5} m$ ; and  $F(e) = (1 - e^2)^{-7/2} (1 + 73e^2/24 + 37e^4/96)$ .

Notice that, by virtue of Kepler’s third law,  $(2\pi G m \omega_{\text{b}} / c^3)^{2/3} = Gm/ac^2 \sim \epsilon$ , thus the first two post-Keplerian parameters can be seen as  $\mathcal{O}(\epsilon)$ , or 1PN corrections to the underlying variable, while the third is an  $\mathcal{O}(\epsilon^{5/2})$ , or 2.5PN correction. The parameters  $r$  and  $s$  are not separately measurable with interesting accuracy for B1913+16 because the orbit’s  $47^{\circ}$  inclination does not lead to a substantial Shapiro delay.

Because  $P_{\text{b}}$  and  $e$  are separately measured parameters, the measurement of the three post-Keplerian parameters provide three constraints on the two unknown masses. The periastron shift measures the total mass of the system,  $\dot{P}_{\text{b}}$  measures the chirp mass, and  $\gamma'$  measures a complicated function of the masses. General relativity passes the test if it provides a consistent solution to these constraints, within the measurement errors.

From the intersection of the  $\langle \dot{\omega} \rangle$  and  $\gamma'$  constraints we obtain the values  $m_1 = 1.4398 \pm 0.0002 M_{\odot}$  and  $m_2 = 1.3886 \pm 0.0002 M_{\odot}$ . The third of Eqs. (29) then predicts the value  $\dot{P}_{\text{b}} = -2.402531 \pm 0.000014 \times 10^{-12}$ . In order to compare the predicted value for  $\dot{P}_{\text{b}}$  with the observed value of Table VI, it is necessary to take into account the small kinematic effect of a relative acceleration between the binary pulsar system and the solar system caused by the differential rotation of the galaxy. Using data on the location and proper motion of the pulsar, combined with the best information available on galactic rotation; the current value of this effect is  $\dot{P}_{\text{b}}^{\text{gal}} \simeq -(0.027 \pm 0.005) \times 10^{-12}$ .

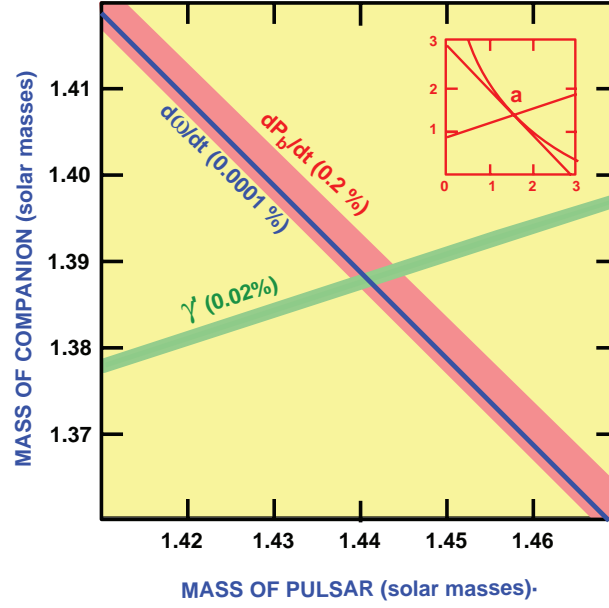


FIG. 5: Constraints on masses of the pulsar and its companion from data on B1913+16, assuming general relativity to be valid. The width of each strip in the plane reflects observational accuracy, shown as a percentage. An inset shows the three constraints on the full mass plane; the intersection region (a) has been magnified 400 times for the full figure.

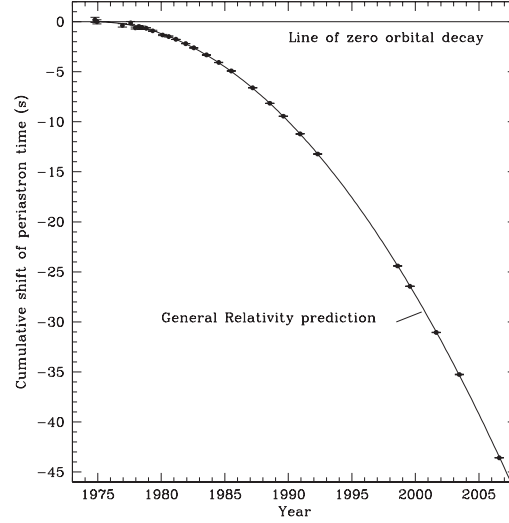


FIG. 6: Plot of the cumulative shift of the periastron time from 1975–2005. The points are data, the curve is the general relativity prediction. The gap during the middle 1990s was caused by a closure of Arecibo for upgrading [90].

Subtracting this from the observed  $\dot{P}_b$  (see Table VI) gives the corrected  $\dot{P}_b^{\text{corr}} = -(2.396 \pm 0.005) \times 10^{-12}$ , which agrees with the prediction within the errors. In other words,

$$\frac{\dot{P}_b^{\text{corr}}}{\dot{P}_b^{\text{GR}}} = 0.997 \pm 0.002. \quad (30)$$

The consistency among the measurements is displayed in Figure 5, in which the regions allowed by the three most precise constraints have a single common overlap. Uncertainties in the parameters that go into the galactic correction are now the limiting factor in the accuracy of the test of gravitational damping.

A third way to display the agreement with general relativity is by plotting the cumulative shift of the time of



periastron passage caused by the changing orbital period. Figure 6 shows the results: the dots are the data points, while the curve is the predicted difference using the measured masses and the quadrupole formula for gravitational radiation damping [90].

The consistency among the constraints provides a test of the assumption that the two bodies behave as “point” masses, without complicated tidal effects, obeying the general relativistic equations of motion including gravitational radiation. It is also a test of strong gravity, in that the highly relativistic internal structure of the neutron stars does not influence their orbital motion, as predicted by the SEP of general relativity.

Observations of variations in the pulse profile suggest that the pulsar is undergoing geodetic precession on a 300-year timescale as it moves through the curved spacetime generated by its companion (see Section VD). The amount is consistent with general relativity, assuming that the pulsar’s spin is suitably misaligned with the orbital angular momentum [92, 93]. Unfortunately, the evidence suggests that the pulsar beam may precess out of our line of sight by 2025.

## B. A zoo of binary pulsars

Over 70 binary neutron star systems with orbital periods less than a day are now known. While some are less interesting for testing relativity, some have yielded interesting tests, and others, notably the recently discovered “double pulsar” are likely to continue to produce significant results well into the future. Here we describe some of the more interesting or best studied cases.

**The “double” pulsar: J0737-3039A, B.** This binary pulsar system, discovered in 2003 [94], was already remarkable for its extraordinarily short orbital period (0.1 days) and large periastron advance ( $16.8995^\circ \text{ yr}^{-1}$ ), but then the companion was also discovered to be a pulsar [95]. Because two projected semi-major axes could be measured, the mass ratio was obtained directly from the ratio of the two values of  $a_p \sin i$ , and thereby the two masses could be obtained by combining that ratio with the periastron advance, assuming general relativity. The results are  $m_A = 1.3381 \pm 0.0007 M_\odot$  and  $m_B = 1.2489 \pm 0.0007 M_\odot$ , where  $A$  denotes the primary (first) pulsar. From these values, one finds that the orbit is nearly edge-on, with  $\sin i = 0.9997$ , a value which is completely consistent with that inferred from the Shapiro delay parameter. In fact, the five measured post-Keplerian parameters plus the ratio of the projected semi-major axes give six constraints on the masses (assuming general relativity): as seen in Fig. 7, all six overlap within their measurement errors [96]. Because of the location of the system, galactic proper motion effects play a significantly smaller role in the interpretation of  $\dot{P}_b$  measurements than they did in B1913+16; this and the reduced effect of interstellar dispersion means that the accuracy of measuring the gravitational-wave damping may soon beat that from the Hulse-Taylor system. The geodetic precession of pulsar B’s spin axis has also been measured by monitoring changes in the patterns of eclipses of the signal from pulsar A, with a result in agreement with general relativity to about 13 percent [97]; the constraint on the masses from that effect (assuming general relativity to be correct) is also shown in Fig. 7.

**J1738+0333: A white-dwarf companion.** This is a low-eccentricity, 8.5-hour period system in which the white-dwarf companion is bright enough to permit detailed spectroscopy, allowing the companion mass to be determined directly to be  $0.181 M_\odot$ . The mass ratio is determined from Doppler shifts of the spectral lines of the companion and of the pulsar period, giving the pulsar mass  $1.46 M_\odot$ . Ten years of observation of the system yielded both a measurement of the apparent orbital period decay, and enough information about its parallax and proper motion to account for the substantial galactic kinematic effect to give a value of the intrinsic period decay of  $\dot{P}_b = (-25.9 \pm 3.2) \times 10^{-15} \text{ s s}^{-1}$  in agreement with the predicted effect [98]. But because of the asymmetry of the system, the result also places a significant bound on the existence of dipole radiation, predicted by many alternative theories of gravity (see Sec. VIC below for discussion). Data from this system were also used to place the tight bound on the PPN parameter  $\alpha_1$  shown in Table IV.

**J1141-6545: A white-dwarf companion.** This system is similar in some ways to the Hulse-Taylor binary: short orbital period (0.20 days), significant orbital eccentricity (0.172), rapid periastron advance (5.3 degrees per year) and massive components ( $M_p = 1.4 M_\odot$ ,  $M_c = 1.0 M_\odot$ ). The key difference is that the companion is again a white dwarf. The intrinsic orbit period decay has been measured in agreement with general relativity to about six percent, again placing limits on dipole gravitational radiation [99].

**J0348+0432: The most massive neutron star.** Discovered in 2011, this is another neutron-star white-dwarf system, in a very short period (0.1 day), low eccentricity ( $2 \times 10^{-6}$ ) orbit. Timing of the neutron star and spectroscopy of the white dwarf have led to mass values of  $0.172 M_\odot$  for the white dwarf and  $2.01 \pm 0.04 M_\odot$  for the pulsar, making it the most massive accurately measured neutron star yet. Along with an earlier measurement of a  $2 M_\odot$  pulsar, this

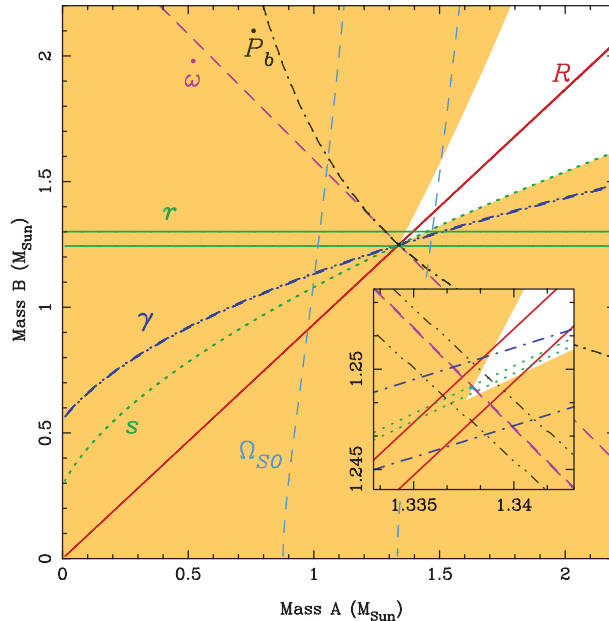


FIG. 7: Constraints on masses of the pulsar and its companion from data on J0737-3039A,B, assuming general relativity to be valid. The inset shows the intersection region magnified by a factor of 80. (Figure courtesy of M. Kramer)

ruled out a number of heretofore viable soft equations of state for nuclear matter. The orbit period decay agrees with the general relativity prediction within 20 percent and is expected to improve steadily with time.

**J0337+1715: Two white-dwarf companions.** This remarkable system was reported in 2014 [76]. It consists of a 2.73 millisecond pulsar ( $M = 1.44 M_{\odot}$ ) with extremely good timing precision, accompanied by *two* white dwarfs in coplanar circular orbits. The inner white dwarf ( $M = 0.1975 M_{\odot}$ ) has an orbital period of 1.629 days, with  $e = 6.918 \times 10^{-4}$ , and the outer white dwarf ( $M = 0.41 M_{\odot}$ ) has a period of 327.26 days, with  $e = 3.536 \times 10^{-2}$ . This is an ideal system for testing the Nordtvedt effect in the strong-field regime. Here the inner system is the analogue of the Earth-Moon system, and the outer white dwarf plays the role of the Sun. Because the outer semi-major axis is about 1/3 of an astronomical unit, the basic driving perturbation is comparable to that provided by the Sun. However, the self-gravitational binding energy per unit mass of the neutron star is almost a billion times larger than that of the Earth, greatly amplifying the size of the Nordtvedt effect. Depending on the details, this system could exceed lunar laser ranging in testing the Nordtvedt effect by several orders of magnitude.

**Other binary pulsars.** Two of the earliest binary pulsars, B1534+12 and B2127+11C, discovered in 1990, failed to live up to their early promise despite being similar to the Hulse-Taylor system in most respects (both were believed to be double neutron-star systems). The main reason was the significant uncertainty in the kinematic effect on  $\dot{P}_b$  of local accelerations, galactic in the case of B1534+12, and those arising from the globular cluster that was home to B2127+11C.

### C. Binary pulsars and alternative theories

Soon after the discovery of the binary pulsar it was widely hailed as a new testing ground for relativistic gravitational effects. As we have seen in the case of general relativity, in most respects, the system has lived up to, indeed exceeded, the early expectations.

In another respect, however, the system has only partially lived up to its promise, namely as a direct testing ground for alternative theories of gravity. The origin of this promise was the discovery that alternative theories of gravity generically predict the emission of dipole gravitational radiation from binary star systems. In general relativity, there is no dipole radiation because the “dipole moment” (center of mass) of isolated systems is uniform in time

(conservation of momentum), and because the “inertial mass” that determines the dipole moment is the same as the mass that generates gravitational waves (SEP). In other theories, while the inertial dipole moment may remain uniform, the “gravity wave” dipole moment need not, because the mass that generates gravitational waves depends differently on the internal gravitational binding energy of each body than does the inertial mass (violation of SEP).

In theories that violate SEP, the difference between gravitational wave mass and inertial mass is a function of the internal gravitational binding energy of the bodies. This additional form of gravitational radiation damping could, at least in principle, be significantly stronger than the usual quadrupole damping, because it depends on fewer powers of the orbital velocity  $v$ , and it depends on the gravitational binding energy per unit mass of the bodies, which, for neutron stars, could be as large as 20 percent (see TEGP 10 for further details). As one fulfillment of this promise, Will and Eardley worked out in detail the effects of dipole gravitational radiation in the bimetric theory of Rosen, and, when the first observation of the decrease of the orbital period was announced in 1979, the Rosen theory suffered a terminal blow. A wide class of alternative theories also failed the binary pulsar test because of dipole gravitational radiation (TEGP 12.3).

On the other hand, the early observations of PSR 1913+16 already indicated that, in general relativity, the masses of the two bodies were nearly equal, so that, in theories of gravity that are in some sense “close” to general relativity, dipole gravitational radiation would not be a strong effect, because of the apparent symmetry of the system. Thus, despite the presence of dipole gravitational radiation, the Hulse–Taylor binary pulsar provides at present only a weak test of Brans–Dicke theory, not competitive with solar-system tests.

However, in some generalized scalar-tensor theories, the strong internal gravity of the neutron star can induce a phenomenon called “spontaneous scalarization” whereby the behavior can be significantly different from either general relativity or from a scalar-tensor theory with a nominally large value of  $\omega_0$ . This is true of theories with negative values of the parameter  $\beta_0$  in Eq. (10) [100]. Furthermore, the recently discovered mixed binary pulsar systems J1141-6545 and J1738+0333 have been exploited using precise timing of the pulsar, spectroscopic observations of the white-dwarf companion, and the strong dipole gravitational radiation effect to yield stringent bounds. Indeed, the latter system surpasses the Cassini bound for  $\beta_0 > 1$  and  $\beta_0 < -2$ , and is close to that bound for the pure Brans–Dicke case  $\beta_0 = 0$  [98].

## VII. TESTING GENERAL RELATIVITY IN ITS SECOND CENTURY

### A. Gravitational-wave tests

Shortly after the centenary year of general relativity, a new opportunity for testing relativistic gravity will be realized, when a worldwide network of advanced kilometer-scale, laser interferometric gravitational wave observatories in the U.S. (LIGO project), and Europe (VIRGO and GEO600 projects), begins regular detection and analysis of gravitational wave signals from astrophysical sources. These will be followed by advanced detectors in Japan and India. They will have the capability of detecting and measuring the gravitational waveforms from astronomical sources in a frequency band between about 10 Hz and 5000 Hz, with a maximum sensitivity to strain at around a hectahertz (100 Hz). The most promising source for detection and study of the gravitational wave signal is the “inspiralling compact binary” – a binary system of neutron stars or black holes (or one of each) in the final minutes of a death spiral leading to a violent merger. Such is the fate, for example, of the Hulse–Taylor binary pulsar B1913+16 in about 300 Myr, or the “double pulsar” J0737-3039 in about 85 Myr. Given the expected sensitivity of “advanced LIGO” (around 2016), which could see such sources out to many hundreds of megaparsecs, it has been estimated that from 10 to several hundred annual inspiral events could be detectable. Other sources, such as binary black-hole mergers, supernova core collapse events, instabilities in rapidly rotating newborn neutron stars, signals from non-axisymmetric pulsars, and a stochastic background of waves, may be detectable. For a review of gravitational-wave theory and detection, see [101].

In addition, plans are being developed for an orbiting laser interferometer space antenna. Such a system, consisting of three spacecraft orbiting the sun in a triangular formation separated from each other by a million kilometers, would be sensitive primarily in the very low frequency band between  $10^{-4}$  and  $10^{-1}$  Hz [102]. Such a mission, dubbed eLISA, is a leading candidate to address the “gravitational universe” science theme that has been selected by the European Space Agency for a mission to be launched around 2034.

A third approach that focuses on the ultra low-frequency band (nanohertz) is that of Pulsar Timing Arrays (PTA), whereby a network of highly stable millisecond pulsars is monitored in a coherent way using radio telescopes, in hopes of detecting the fluctuations in arrival times induced by passing gravitational waves.

In addition to opening a new astronomical window, the detailed observation of gravitational waves by such observatories may provide the means to test general relativistic predictions for the polarization and speed of the waves, for gravitational radiation damping and for strong-field gravity.

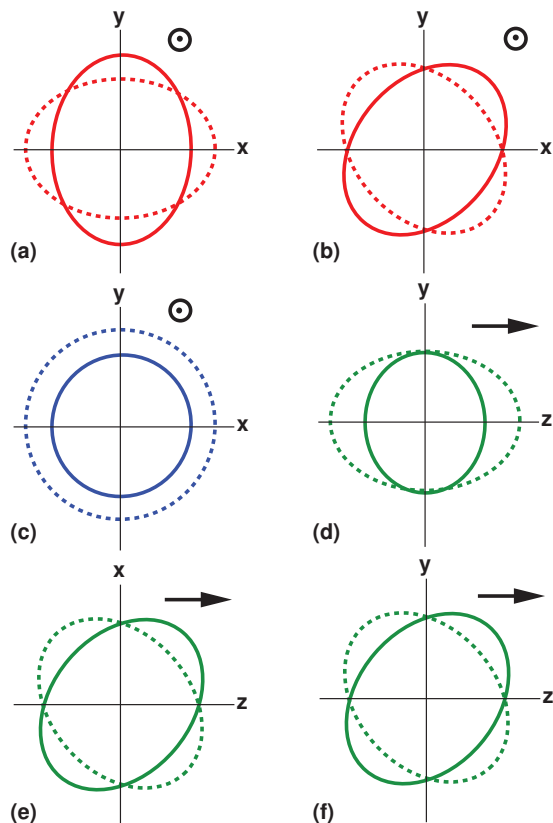


FIG. 8: The six polarization modes for gravitational waves permitted in any metric theory of gravity. Shown is the displacement that each mode induces on a ring of test particles. The wave propagates in the  $+z$  direction. There is no displacement out of the plane of the picture. In (a), (b), and (c), the wave propagates out of the plane; in (d), (e), and (f), the wave propagates in the plane.

### 1. Polarization of gravitational waves

Like electromagnetic waves, gravitational waves can be characterized by polarizations. In general metric theories of gravity there are six independent polarization modes. Three are transverse to the direction of propagation, with two representing quadrupolar deformations and one representing a monopolar “breathing” deformation. Three modes are longitudinal, with one an axially symmetric stretching mode in the propagation direction, and one quadrupolar mode in each of the two orthogonal planes containing the propagation direction. Figure 8 shows the displacements induced on a ring of freely falling test particles by each of these modes. General relativity predicts only the first two transverse quadrupolar modes (a) and (b) independently of the source. Massless scalar-tensor gravitational waves can in addition contain the transverse breathing mode (c). More general metric theories predict additional longitudinal modes, up to the full complement of six (TEGP 10.2).

A suitable array of gravitational antennas could delineate or limit the number of modes present in a given wave; a space antenna could do likewise by virtue of its changing orientation during the passage of a sufficiently long wave train. If distinct evidence were found of any mode other than the two transverse quadrupolar modes of general relativity, the result would be disastrous for general relativity.

### 2. Gravitational radiation back-reaction

In the binary pulsar, a test of general relativity was made possible by measuring at least three relativistic effects that depended upon only two unknown masses. The evolution of the orbital phase under the damping effect of gravitational radiation played a crucial role. Another situation in which measurement of orbital phase can lead to tests of general relativity is that of the inspiralling compact binary system. The key differences are that here gravitational radiation itself is the detected signal, rather than radio pulses, and the phase evolution alone carries all the information. In the

binary pulsar, the first derivative of the binary frequency  $\dot{\omega}_b$  was measured; here the full nonlinear variation of  $\omega_b$  as a function of time is measured.

Broad-band laser interferometers are especially sensitive to the phase evolution of the gravitational waves, which carry the information about the orbital phase evolution. The analysis of gravitational wave data from such sources will involve some form of matched filtering of the noisy detector output against an ensemble of theoretical “template” waveforms which depend on the intrinsic parameters of the inspiralling binary, such as the component masses, spins, and so on, and on its inspiral evolution.

But for laser interferometric observations of gravitational waves, the bottom line is that, in order to measure the astrophysical parameters of the source and to test the properties of the gravitational waves, it is necessary to derive the gravitational waveform and the resulting radiation back-reaction on the orbit phasing to many post-Newtonian orders beyond the quadrupole approximation. Two decades of intensive work by many groups have led to the development of waveforms in general relativity that are accurate to 3.5PN order, and for some specific effects, such as those related to spin, to 4.5PN order (see [103] for a thorough review).

On the other hand, alternative theories of gravity are likely to predict rather different gravitational waveforms, notably via the addition of dipole gravitational radiation. Thus tests of alternative theories might be possible using the gravitational-wave signals. Several attempts have been made to parametrize the gravitational-wave signal from binary inspiral, in order to encompass alternative theories of gravity, in the spirit of the PPN framework [104, 105].

### 3. Speed of gravitational waves

According to general relativity, in the limit in which the wavelength of gravitational waves is small compared to the radius of curvature of the background spacetime, the waves propagate along null geodesics of the background spacetime, i.e. they have the same speed  $c$  as light (in this section, we do not set  $c = 1$ ). In other theories, the speed could differ from  $c$  because of coupling of gravitation to other gravitational fields, or if gravitation were propagated by a massive field (a massive graviton). In the latter case  $v_g$  would be given by, in a local inertial frame,

$$\frac{v_g^2}{c^2} = 1 - \frac{m_g^2 c^4}{E^2}, \quad (31)$$

where  $m_g$  and  $E$  are the graviton rest mass and energy, respectively.

The most obvious way to test this is to compare the arrival times of a gravitational wave and an electromagnetic wave from the same event, e.g., a supernova, or a binary inspiral with an associated electromagnetic signal. For a source at a distance  $D$ , the resulting value of the difference  $1 - v_g/c$  is

$$1 - \frac{v_g}{c} = 5 \times 10^{-17} \left( \frac{200 \text{ Mpc}}{D} \right) \left( \frac{\Delta t}{1 \text{ s}} \right), \quad (32)$$

where  $\Delta t \equiv \Delta t_a - (1 + Z)\Delta t_e$  is the “time difference”, where  $\Delta t_a$  and  $\Delta t_e$  are the differences in arrival time and emission time of the two signals, respectively, and  $Z$  is the redshift of the source. In many cases,  $\Delta t_e$  is unknown, so that the best one can do is employ an upper bound on  $\Delta t_e$  based on observation or modelling. The result will then be a bound on  $1 - v_g/c$ .

The foregoing discussion assumes that the source emits *both* gravitational and electromagnetic radiation in detectable amounts, and that the relative time of emission can be established to sufficient accuracy, or can be shown to be sufficiently small.

However, there is a situation in which a bound on the graviton mass can be set using gravitational radiation alone [106]. That is the case of the inspiralling compact binary. Because the frequency of the gravitational radiation sweeps from low frequency at the initial moment of observation to higher frequency at the final moment, the speed of the gravitons emitted will vary, from lower speeds initially to higher speeds (closer to  $c$ ) at the end. This will cause a distortion of the observed phasing of the waves that can be detected or bounded through matched filtering.

These and other tests of gravitational theory using gravitational waves are thoroughly reviewed by [107] and by [108].

## B. Strong-field tests

One of the central difficulties of testing general relativity in the strong-field regime is the possibility of contamination by uncertain or complex physics. In the solar system, weak-field gravitational effects can in most cases be measured cleanly and separately from non-gravitational effects. The remarkable cleanliness of binary pulsars permits precise measurements of gravitational phenomena in a partially strong-field context.

Unfortunately, nature is rarely so kind. Still, under suitable conditions, qualitative and even quantitative strong-field tests of general relativity could be carried out.

One example is the exploration of the spacetime near black holes and neutron stars. Studies of certain kinds of accretion known as advection-dominated accretion flow (ADAF) in low-luminosity binary X-ray sources may yield the signature of the black hole event horizon [109]. The spectrum of frequencies of quasi-periodic oscillations (QPO) from galactic black hole binaries may permit measurement of the spins of the black holes [110]. Aspects of strong-field gravity and frame-dragging may be revealed in spectral shapes of iron fluorescence lines from the inner regions of accretion disks [111, 112]. Using submm VLBI, a collaboration dubbed the Event Horizon Telescope could image our galactic center black hole SgrA\* and the black hole in M87 with horizon-scale angular resolution; observation of accretion phenomena at these angular resolutions could provide tests of the spacetime geometry very close to the black hole [113]. Tracking of hypothetical stars whose orbits are within a fraction of a milliparsec of SgrA\* could test the black hole “ho-hair” theorem, via a direct measurement of both the angular momentum  $J$  and quadrupole moment  $Q$  of the black hole, and a test of the requirement that  $Q = -J^2/M$  [114].

Because of uncertainties in the detailed models, the results to date of studies like these are suggestive at best, but the combination of future higher-resolution observations and better modelling could lead to striking tests of strong-field predictions of general relativity.

For a detailed review of strong-field tests of general relativity using electromagnetic observations, see [115].

## VIII. CONCLUSIONS

General relativity has held up under extensive experimental scrutiny. The question then arises, why bother to continue to test it? One reason is that gravity is a fundamental interaction of nature, and as such requires the most solid empirical underpinning we can provide. Another is that all attempts to quantize gravity and to unify it with the other forces suggest that the standard general relativity of Einstein may not be the last word. Furthermore, the predictions of general relativity are fixed; the pure theory contains no adjustable constants so nothing can be changed. Thus every test of the theory is either a potentially deadly test or a possible probe for new physics. Although it is remarkable that this theory, born 100 years ago out of almost pure thought, has managed to survive every test, the possibility of finding a discrepancy will continue to drive experiments for years to come. These experiments will search for new physics beyond Einstein at many different scales: the large distance scales of the astrophysical, galactic, and cosmological realms; scales of very short distances or high energy; and scales related to strong or dynamical gravity.

Having spent almost half of the century of general relativity’s existence being astonished by its continuing agreement with observation, I might be permitted a personal reflection at this point on the future of the subject: *It would not at all surprise me if general relativity turned out to be perfectly valid at all scales, from the cosmological to the astrophysical to the microscopic, failing only at the Planck scale where one naturally expects quantum gravity to take over.*

Of course, having made that statement, I am reminded of the story about Yogi Berra, the famous New York Yankees baseball player and manager (one of my childhood heroes), and one blessed with the most sublimely illogical mind. At some point after his retirement from baseball, his wife Carmen asked him: “Yogi, you were born in St. Louis, you played ball in New York and we now live in New Jersey. If you should die first, where would you like me to bury you?” Yogi’s answer: “Surprise me!”

## Acknowledgments

This work was supported in part by the National Science Foundation, Grant Numbers PHY 12-60995 and 13-06069. I am grateful for the hospitality of the Institut d’Astrophysique de Paris, where this article was prepared.

- 
- [1] C. Will, *Was Einstein Right?: Putting General Relativity to the Test* (Basic Books, New York, 1993), 2nd ed.
  - [2] C. Will, *Theory and Experiment in Gravitational Physics* (Cambridge University Press, Cambridge; New York, 1993), 2nd ed.
  - [3] C. Will, Living Rev. Relativity **9** (2006), <http://www.livingreviews.org/lrr-2006-3>.
  - [4] C. Will, Living Rev. Relativity **17** (2014), <http://www.livingreviews.org/lrr-2014-4>.
  - [5] C. Will, Am. J. Phys. **78**, 1240 (2010), 1008.0296.
  - [6] R. Dicke, in *Relativity, Groups and Topology*, edited by C. DeWitt and B. DeWitt (Gordon and Breach, New York; London, 1964), pp. 165–313.

- [7] S. Schlamminger, K.-Y. Choi, T. A. Wagner, J. H. Gundlach, and E. G. Adelberger, *Phys. Rev. Lett.* **100**, 041101 (2008), 0712.0607.
- [8] S. Merlet, Q. Bodart, N. Malossi, A. Landragin, F. Pereira Dos Santos, O. Gitlein, and L. Timmen, *Metrologia* **47**, L9 (2010), 1005.0357.
- [9] H. Müller, A. Peters, and S. Chu, *Nature* **463**, 926 (2010).
- [10] P. Wolf, L. Blanchet, C. J. Bordé, S. Reynaud, C. Salomon, and C. Cohen-Tannoudji, *Class. Quantum Grav.* **28**, 145017 (2011), 1012.1194.
- [11] J. M. Hogan, D. M. S. Johnson, and M. A. Kasevich, in *Atom Optics and Space Physics: Proceedings of the International School of Physics "Enrico Fermi", Course 168*, edited by E. Arimondo, W. Ertmer, W. P. Schleich, and E. M. Raseel (IOS Press Amsterdam, 2009), p. 411, 0806.3261.
- [12] E. Fischbach, G. Gillies, D. Krause, J. Schwan, and C. Talmadge, *Metrologia* **29**, 213 (1992).
- [13] C. Speake and C. Will, *Class. Quantum Grav.* **29**, 180301 (2012), URL <http://stacks.iop.org/0264-9381/29/i=18/a=180301>.
- [14] E. G. Adelberger, J. H. Gundlach, B. R. Heckel, S. Hoedl, and S. Schlamminger, *Prog. Part. Nucl. Phys.* **62**, 102 (2009).
- [15] C. Will, in *Einstein, 1905-2005: Poincaré Seminar 2005*, edited by T. Damour, O. Darrigol, B. Duplantier, and V. Rivasseau (Birkhäuser Verlag, Basel, 2006), p. 33.
- [16] D. Mattingly, *Living Rev. Relativity* **8**, lrr-2005-5 (2005), <http://www.livingreviews.org/lrr-2005-5>, gr-qc/0502097.
- [17] S. Liberati, *Class. Quantum Grav.* **30**, 133001 (2013), URL <http://stacks.iop.org/0264-9381/30/i=13/a=133001>.
- [18] V. Kostelecký and N. Russell, *Rev. Mod. Phys.* **83**, 11 (2011), URL <http://link.aps.org/doi/10.1103/RevModPhys.83.11>.
- [19] V. Kostelecký and J. Tasson, *Phys. Rev. D* **83**, 016013 (2011), URL <http://link.aps.org/doi/10.1103/PhysRevD.83.016013>.
- [20] J. LoPresto, C. Schrader, and A. Pierce, *Astrophys. J.* **376**, 757 (1991).
- [21] J. Guéna, M. Abgrall, D. Rovera, P. Rosenbusch, M. E. Tobar, P. Laurent, A. Clairon, and S. Bize, *Phys. Rev. Lett.* **109**, 080801 (2012), 1205.4235.
- [22] S. Peil, S. Crane, J. L. Hanssen, T. B. Swanson, and C. R. Ekstrom, *Phys. Rev. A* **87**, 010102 (2013), 1301.6145.
- [23] N. Leefer, C. T. M. Weber, A. Cingöz, J. R. Torgerson, and D. Budker, *Phys. Rev. Lett.* **111**, 060801 (2013), 1304.6940.
- [24] N. Ashby, *Living Rev. Relativity* **6**, lrr-2003-1 (2003), <http://www.livingreviews.org/lrr-2003-1>.
- [25] C. Will, *Einstein's relativity and everyday life* (2000), <http://www.physicscentral.com/writers/writers-00-2.html>.
- [26] F. Dyson, in *Aspects of Quantum Theory*, edited by A. Salam and E. Wigner (Cambridge University Press, Cambridge; New York, 1972), pp. 213–236.
- [27] J.-P. Uzan, *Living Rev. Relativity* **14** (2011), <http://www.livingreviews.org/lrr-2011-2>, 1009.5514.
- [28] J. A. King, J. K. Webb, M. T. Murphy, V. V. Flambaum, R. F. Carswell, M. B. Bainbridge, M. R. Wilczynska, and F. E. Koch, *Mon. Not. R. Astron. Soc.* **422**, 3370 (2012), 1202.4758.
- [29] N. Kanekar, G. I. Langston, J. T. Stocke, C. L. Carilli, and K. M. Menten, *Astrophys. J. Lett.* **746**, L16 (2012), 1201.3372.
- [30] L. Lentati, C. Carilli, P. Alexander, R. Maiolino, R. Wang, P. Cox, D. Downes, R. McMahon, K. M. Menten, R. Neri, et al., *Mon. Not. R. Astron. Soc.* **430**, 2454 (2013), 1211.3316.
- [31] S. G. Turyshev and V. T. Toth, *Living Rev. Relativity* **13**, lrr-2010-4 (2010), <http://www.livingreviews.org/lrr-2010-4>, 1001.3686.
- [32] S. G. Turyshev, V. T. Toth, G. Kinsella, S.-C. Lee, S. M. Lok, and J. Ellis, *Phys. Rev. Lett.* **108**, 241101 (2012), 1204.2507.
- [33] B. Schutz, *A First Course in General Relativity* (Cambridge University Press, Cambridge, 2009).
- [34] E. Poisson and C. Will, *Gravity: Newtonian, Post-Newtonian, Relativistic* (Cambridge University Press, Cambridge, 2014).
- [35] K. Nordtvedt Jr., *Phys. Rev.* **169**, 1017 (1968).
- [36] C. Will, *Astrophys. J.* **163**, 611 (1971).
- [37] C. Will and K. Nordtvedt Jr., *Astrophys. J.* **177**, 757 (1972).
- [38] C. Misner, K. Thorne, and J. Wheeler, *Gravitation* (W.H. Freeman, San Francisco, 1973).
- [39] T. Damour and G. Esposito-Farèse, *Class. Quantum Grav.* **9**, 2093 (1992).
- [40] T. Damour and K. Nordtvedt Jr., *Phys. Rev. Lett.* **70**, 2217 (1993).
- [41] T. Damour and K. Nordtvedt Jr., *Phys. Rev. D* **48**, 3436 (1993).
- [42] Y. Fujii and K.-I. Maeda, *The Scalar-Tensor Theory of Gravitation* (Cambridge University Press, Cambridge, 2007).
- [43] T. P. Sotiriou and V. Faraoni, *Rev. Mod. Phys.* **82**, 451 (2010), 0805.1726.
- [44] A. De Felice and S. Tsujikawa, *Living Rev. Relativity* **13** (2010), <http://www.livingreviews.org/lrr-2010-3>, URL <http://www.living\discretionary{-}{-}{-}reviews.\discretionary{-}{-}{-}org/lrr-2010-3>.
- [45] R. Hellings and K. Nordtvedt Jr., *Phys. Rev. D* **7**, 3593 (1973).
- [46] T. Jacobson and D. Mattingly, *Phys. Rev. D* **64**, 024028 (2001), gr-qc/0007031.
- [47] D. Mattingly and T. Jacobson, in *CPT and Lorentz Symmetry II*, edited by V. Kostelecký (World Scientific, Singapore; River Edge, 2002), pp. 331–335, gr-qc/0112012.
- [48] T. Jacobson and D. Mattingly, *Phys. Rev. D* **70**, 024003 (2004), gr-qc/0402005.
- [49] C. Eling and T. Jacobson, *Phys. Rev. D* **69**, 064005 (2004), gr-qc/0310044.
- [50] B. Foster and T. Jacobson, *Phys. Rev. D* **73**, 064015 (2006), gr-qc/0509083.
- [51] P. Hořava, *Phys. Rev. D* **79**, 084008 (2009), 0901.3775.
- [52] D. Blas, O. Pujolàs, and S. Sibiryakov, *Phys. Rev. Lett.* **104**, 181302 (2010), 0909.3525.
- [53] D. Blas, O. Pujolàs, and S. Sibiryakov, *J. High Energy Phys.* **4**, 18 (2011), 1007.3503.
- [54] T. Jacobson, *Phys. Rev. D* **89**, 081501 (2014), 1310.5115.
- [55] J. D. Bekenstein, *Phys. Rev. D* **70**, 083509 (2004), URL <http://link.aps.org/doi/10.1103/PhysRevD.70.083509>.

- [56] C. Skordis, Phys. Rev. D **77**, 123502 (2008), URL <http://link.aps.org/doi/10.1103/PhysRevD.77.123502>.
- [57] E. Sagi, Phys. Rev. D **80**, 044032 (2009), URL <http://link.aps.org/doi/10.1103/PhysRevD.80.044032>.
- [58] C. Skordis, Class. Quantum Grav. **26**, 143001 (2009), 0903.3602.
- [59] B. Famaey and S. S. McGaugh, Living Rev. Relativity **15** (2012), <http://www.livingreviews.org/lrr-2012-10>, 1112.3960.
- [60] K. Hinterbichler, Rev. Mod. Phys. **84**, 671 (2012), 1105.3735.
- [61] C. Will, Am. J. Phys. **56**, 413 (1988).
- [62] S. Shapiro, J. Davis, D. Lebach, and J. Gregory, Phys. Rev. Lett. **92**, 121101 (2004).
- [63] S. B. Lambert and C. Le Poncin-Lafitte, Astron. Astrophys. **529**, A70 (2011).
- [64] A. S. Bolton, S. Rappaport, and S. Burles, Phys. Rev. D **74**, 061501 (2006), arXiv:astro-ph/0607657.
- [65] B. Bertotti, L. Iess, and P. Tortora, Nature **425**, 374 (2003).
- [66] A. Fienga, J. Laskar, P. Kuchynka, H. Manche, G. Desvignes, M. Gastineau, I. Cognard, and G. Theureau, Cel. Mech. Dyn. Astron. **111**, 363 (2011), 1108.5546.
- [67] A. K. Verma, A. Fienga, J. Laskar, H. Manche, and M. Gastineau, Astron. Astrophys. **561**, A115 (2014), 1306.5569.
- [68] D. M. Lucchesi and R. Peron, Phys. Rev. D **89**, 082002 (2014).
- [69] K. Nordtvedt Jr., Phys. Rev. **169**, 1014 (1968).
- [70] R. Dicke, *Gravitation and the universe*, vol. 78 of *Memoirs of the American Philosophical Society. Jayne Lecture for 1969* (American Philosophical Society, Philadelphia, 1970).
- [71] S. M. Merkowitz, Living Rev. Relativity **13** (2010), <http://www.livingreviews.org/lrr-2010-7>.
- [72] J. Williams, S. Turyshev, and T. Murphy Jr, Int. J. Mod. Phys. D **13**, 567 (2004), gr-qc/0311021.
- [73] S. Baeßler, B. Heckel, E. Adelberger, J. Gundlach, U. Schmidt, and H. Swanson, Phys. Rev. Lett. **83**, 3585 (1999).
- [74] T. W. Murphy, Jr., E. G. Adelberger, J. B. R. Battat, C. D. Hoyle, N. H. Johnson, R. J. McMillan, C. W. Stubbs, and H. E. Swanson, Class. Quantum Grav. **29**, 184005 (2012).
- [75] I. Stairs, A. Faulkner, A. Lyne, M. Kramer, D. Lorimer, M. McLaughlin, R. Manchester, G. Hobbs, F. Camilo, A. Possenti, et al., Astrophys. J. **632**, 1060 (2005), astro-ph/0506188.
- [76] S. M. Ransom, I. H. Stairs, A. M. Archibald, J. W. T. Hessels, D. L. Kaplan, M. H. van Kerkwijk, J. Boyles, A. T. Deller, S. Chatterjee, A. Schechtman-Rook, et al., Nature (London) **505**, 520 (2014), 1401.0535.
- [77] L. Shao and N. Wex, Class. Quantum Grav. **29**, 215018 (2012), 1209.4503.
- [78] L. Shao, R. N. Caballero, M. Kramer, N. Wex, D. J. Champion, and A. Jessner, Class. Quantum Grav. **30**, 165019 (2013), 1307.2552.
- [79] L. Shao and N. Wex, Class. Quantum Grav. **30**, 165020 (2013), 1307.2637.
- [80] A. S. Konopliv, S. W. Asmar, W. M. Folkner, Ö. Karatekin, D. C. Nunes, S. E. Smrekar, C. F. Yoder, and M. T. Zuber, Icarus **211**, 401 (2011).
- [81] J. Williams, S. Turyshev, and D. Boggs, Phys. Rev. Lett. **93**, 261101 (2004), gr-qc/0411113.
- [82] A. T. Deller, J. P. W. Verbiest, S. J. Tingay, and M. Bailes, Astrophys. J. Lett. **685**, L67 (2008), 0808.1594.
- [83] K. Lazaridis, N. Wex, A. Jessner, M. Kramer, B. W. Stappers, G. H. Janssen, G. Desvignes, M. B. Purver, I. Cognard, G. Theureau, et al., Mon. Not. R. Astron. Soc. **400**, 805 (2009), 0908.0285.
- [84] D. Guenther, L. Krauss, and P. Demarque, Astrophys. J. **498**, 871 (1998).
- [85] C. Copi, A. Davis, and L. Krauss, Phys. Rev. Lett. **92**, 171301 (2004), astro-ph/0311334.
- [86] C. Bambi, M. Giannotti, and F. Villante, Phys. Rev. D **71**, 123524 (2005), astro-ph/0503502.
- [87] C. W. F. Everitt, D. B. Debra, B. W. Parkinson, J. P. Turneure, J. W. Conklin, M. I. Heifetz, G. M. Keiser, A. S. Silbergleit, T. Holmes, J. Kolodziejczak, et al., Phys. Rev. Lett. **106**, 221101 (2011), 1105.3456.
- [88] I. Ciufolini and E. Pavlis, Nature **431**, 958 (2004).
- [89] I. Ciufolini, E. C. Pavlis, and R. Peron, New Astronomy **11**, 527 (2006).
- [90] J. M. Weisberg, D. J. Nice, and J. H. Taylor, Astrophys. J. **722**, 1030 (2010), 1011.0718.
- [91] T. Damour and J. Taylor, Phys. Rev. D **45**, 1840 (1992).
- [92] M. Kramer, Astrophys. J. **509**, 856 (1998), astro-ph/9808127.
- [93] J. Weisberg and J. Taylor, Astrophys. J. **576**, 942 (2002), astro-ph/0205280.
- [94] M. Burgay, N. D'Amico, A. Possenti, R. Manchester, A. Lyne, B. Joshi, M. McLaughlin, M. Kramer, J. Sarkissian, F. Camilo, et al., Nature **426**, 531 (2003), astro-ph/0312071.
- [95] A. Lyne, M. Burgay, M. Kramer, A. Possenti, R. Manchester, F. Camilo, M. McLaughlin, D. Lorimer, N. D'Amico, B. Joshi, et al., Science **303**, 1153 (2004), astro-ph/0401086.
- [96] M. Kramer, I. H. Stairs, R. N. Manchester, M. A. McLaughlin, A. G. Lyne, R. D. Ferdman, M. Burgay, D. R. Lorimer, A. Possenti, N. D'Amico, et al., Science **314**, 97 (2006), arXiv:astro-ph/0609417.
- [97] R. P. Breton, V. M. Kaspi, M. Kramer, M. A. McLaughlin, M. Lyutikov, S. M. Ransom, I. H. Stairs, R. D. Ferdman, F. Camilo, and A. Possenti, Science **321**, 104 (2008), 0807.2644.
- [98] P. C. C. Freire, N. Wex, G. Esposito-Farèse, J. P. W. Verbiest, M. Bailes, B. A. Jacoby, M. Kramer, I. H. Stairs, J. Antoniadis, and G. H. Janssen, Mon. Not. R. Astron. Soc. **423**, 3328 (2012), 1205.1450.
- [99] N. D. R. Bhat, M. Bailes, and J. P. W. Verbiest, Phys. Rev. D **77**, 124017 (2008), 0804.0956.
- [100] T. Damour and G. Esposito-Farèse, Phys. Rev. D **58**, 042001 (1998), gr-qc/9803031.
- [101] J. Creighton and W. Anderson, *Gravitational-Wave Physics and Astronomy: An Introduction to Theory, Experiment and Data Analysis* (Wiley, Cambridge; New York, 2011).
- [102] P. Amaro-Seoane, S. Aoudia, S. Babak, P. Binétruy, E. Berti, A. Bohé, C. Caprini, M. Colpi, N. J. Cornish, K. Danzmann, et al., Class. Quantum Grav. **29**, 124016 (2012), 1202.0839.



- [103] L. Blanchet, *Living Rev. Relativity* **9** (2006), <http://www.livingreviews.org/lrr-2006-4>.
- [104] N. Yunes and F. Pretorius, *Phys. Rev. D* **80**, 122003 (2009), 0909.3328.
- [105] C. K. Mishra, K. G. Arun, B. R. Iyer, and B. S. Sathyaprakash, *Phys. Rev. D* **82**, 064010 (2010), 1005.0304.
- [106] C. Will, *Phys. Rev. D* **57**, 2061 (1998), gr-qc/9709011.
- [107] J. R. Gair, M. Vallisneri, S. L. Larson, and J. G. Baker, *Living Rev. Relativity* **16** (2013), <http://www.livingreviews.org/lrr-2013-7>, 1212.5575.
- [108] N. Yunes and X. Siemens, *Living Rev. Relativity* **16**, lrr-2013-9 (2013), <http://www.livingreviews.org/lrr-2013-9>, 1304.3473.
- [109] R. Narayan and J. E. McClintock, *New Astron. Rev.* **51**, 733 (2008), 0803.0322.
- [110] D. Psaltis, in *X-Ray Timing 2003: Rossi and Beyond*, edited by P. Kaaret, F. Lamb, and J. Swank (American Institute of Physics, Melville, 2004), vol. 714 of *AIP Conference Proceedings*, pp. 29–35, astro-ph/0402213.
- [111] C. S. Reynolds, *Space Sci. Rev. On Line* pp. 1–18 (2013), 1302.3260, URL <http://adsabs.harvard.edu/abs/2013SSRv...tmp...81R>.
- [112] C. S. Reynolds, *Class. Quantum Grav.* **30**, 244004 (2013), 1307.3246.
- [113] S. Doleman, E. Agol, D. Backer, F. Baganoff, G. C. Bower, A. Broderick, A. Fabian, V. Fish, C. Gammie, P. Ho, et al., in *Astro2010: The Astronomy and Astrophysics Decadal Survey* (2009), p. 68, 0906.3899.
- [114] C. Will, *Astrophys. J. Lett.* **674**, L25 (2008), 0711.1677.
- [115] D. Psaltis, *Living Rev. Relativity* **11** (2008), <http://www.livingreviews.org/lrr-2008-9>, 0806.1531.